Acta Geochim
https://doi.org/10.1007/s11631-020-00404-8

ORIGINAL ARTICLE

Geotectonic significance of the Neoproterozoic ophiolitic metagabbros of Muiswirab area, South Eastern Desert, Egypt: constraints from their mineralogical and geochemical characteristics

Moustafa M. Mogahed[1] · Wlaa Mahmoud Saad[1]

Received: 14 September 2019 / Revised: 3 January 2020 / Accepted: 29 January 2020
© Science Press and Institute of Geochemistry, CAS and Springer-Verlag GmbH Germany, part of Springer Nature 2020

Abstract Petrological and geochemical studies of Neoproterozoic metagabbros were carried out in the Muiswirab area, South Eastern Desert of Egypt. The Muiswirab area comprises of ophiolitic metagabbroic rocks (MOM), which are tectonically thrusted over a thick pile of metavolcanic rocks and intruded by syn- and post-tectonic granitoid rocks. The whole-rock geochemical variations coupled with chemical compositions of mineral constituents are used to attain the genesis and tectonic evolution of the studied metagabbros. The geothermobarometric investigation of the analyzed amphiboles from (MOM) revealed that these metagabbros underwent regional metamorphism under lower to upper greenschist facies (biotite zone) conditions (at a temperature of 450 to 500 °C and pressure of 1–3 kbar). Geochemically, the metagabbros (MOM) show tholeiitic affinity and exhibiting both arc- and MORB- like characters as evidenced by their clinopyroxene compositions and the Ti/V ratios (11.84–31.65), which considered as prominent features of forearc tectonic regime. The geochemical features suggest a probable fractionation of olivine ± clinopyroxene ± plagioclase as well as insignificant crustal contamination. The parental magma of the investigated MOM rocks seems to be developed in a sub-arc mantle wedge setting due to the enrichments of LILE (e.g., Rb, Ba, Sr, Pb) over HFSE (e.g., Ti, Nb, Y, Zr, Hf, Ta). The studied MOM rocks have lower values of Nb/U relative to MORB and OIB indicating that their geochemical variation produced due to the enrichment of a lithosphere mantle by OIB-like components. The ratios of Zn/Fet, La/Sm, Sm/Yb, Th/Yb and Nb/Yb indicate that the MOM rocks represent a fragment of oceanic crust originated at a supra-subduction zone environment and their parental magma developed by 5–30 % partial melting of a spinel lherzolite mantle rather than pyroxenite in an island arc setting and conformable with most of the Egyptian ophiolitic metagabbros.

Keywords Egypt · Eastern Desert · Muiswirab area · Ophiolitic metagabbros · N-MORB · Arc tholeiites · Forearc tectonic regime · Volcanic-arc setting

1 Introduction

The characteristics and origin of oceanic island arcs rocks attract considerable attention. Most studies have focused on volcanic rocks, as volcanic rocks constitute most of the exposed oceanic island arc rocks. Although the plutonic rocks—which make up at least 10 % of the exposed igneous assemblage—represent the exposed roots of oceanic island arcs and are generally more quartz-rich than the volcanic rocks, they have received markedly little attention. Generally, plutonic rocks of oceanic island arcs are comprised of gabbros and granitoids. The studying of such rocks provides valuable opportunity for detecting their characterization and origin (Kawate and Arima 1998; Saito et al. 2004; Jagoutz et al. 2009) and represent the clue to understanding the processes occurring at depth, as well as the tectonic setting of the oceanic and continental crusts (e.g., Rudnick and Gao 2003; Jagoutz et al. 2009).

Electronic supplementary material The online version of this article (https://doi.org/10.1007/s11631-020-00404-8) contains supplementary material, which is available to authorized users.

✉ Moustafa M. Mogahed
mustafa.ahmed01@fsc.bu.edu.eg

[1] Geology Department, Faculty of Science, Benha University-Egypt, P.O. Box 13518, Benha, Egypt

Published online: 06 February 2020

The crustal evolution of the Arabo-Nubian shield (ANS) is currently interpreted within the framework of plate tectonics. This shield is one of the best-documented examples of the Pan-African (Late Proterozoic) crustal growth through processes of island-arc accretion, where ophiolites represent characteristic features of the Pan-African orogenic belt of the ANS (El Ramly et al. 1993; Abdel-Karim and Ahmed 2010; Ali et al. 2010; Abdel-Karim et al. 2018; Stern 2018).

The Neoproterozoic basement rocks of Egypt represent the northwestern extension portion of the (ANS). They approximately cover the whole Eastern Desert, which extended southward to the Red Sea Hills of northern Sudan. Gneissic core complexes, ophiolites, volcano-sedimentary successions, and granitoid intrusions represent the main lithologic units of the basement complex of the Egyptian Eastern Desert (e.g. Stern 2018).

The Egyptian Precambrian gabbroic rocks were classified as older and younger gabbros (Akaad and Noweir 1980; Takla et al. 1981). The latter is metamorphosed and agreed to be post tectonic intrusions, being younger than Hammamat group since it does contain any boulders of fresh gabbro (El Ramly 1972). El-Gaby (2007), differentiated the Egyptian gabbros into three groups including; ophiolitic metagabbros with tholeiitic affinity, metamorphosed intrusive subduction-related calc-alkaline gabbros, and within-plate layered olivine gabbro intrusion. It is hard to differentiate between ophiolitic metagabbros and island-arc metagabbros as both are regionally metamorphosed up to the lower amphibolite facies (Abu El-Ela 1997; Ali et al. 2010).

Ophiolites are widely distributed through the ANS ranging in age from 870 to 627 Ma (Dilek and Ahmed 2003; Stern et al. 2004). Neoproterozoic ophiolitic rocks are abundant in the central and southern portions of the Egyptian Eastern Desert (Fig. 1a). Geochronological studies revealed that the age of the Egyptian ophiolites ranging from (690–890 Ma; mean = 781 ± 47 Ma, Stern et al. 2004). Zimmer et al. (1995) stated that the Egyptian ophiolite were emplaced over an interval of ∼ 105 Ma. In addition, the ages of the Egyptian ophiolites overlap with the island arc stage of ANS development (∼ 770 to ∼ 720 Ma; Stern and Hedge 1985). The ophiolitic metagabbros of Gabal Gerf, South Eastern Desert, Egypt (Fig. 1a) have 720 ± 9 Ma Sm/Nd age while they show a rather older age of about (770 ± 52 Ma) based on their clinopyroxene and plagioclase minerals (Zimmer et al. 1995).

Although the ANS ophiolites have been carried out by a great deal of work, their origin and tectonic setting are still debated. There is a general agreement that ANS ophiolites exhibiting supra-subduction zone (SSZ) geochemical signatures. However, controversy exists on whether they are formed in back-arc (e.g., El-Sayed et al. 1999; Farahat et al. 2004; Abd El-Rahman et al. 2009) or forearc settings (e.g., Stern et al. 2004; Azer and Stern 2007; Abd El-Rahman et al. 2009; Farahat et al. 2011; Obeid et al. 2016; Mogahed 2019). Most ophiolites may include both MOR- and island arc-types due to the multistage histories of the ophiolite (e.g., Portnyagin et al. 1997; Pearce et al. 2000; Dilek and Ahmed 2003; Flower and Dilek 2003; Saccani and Photiades 2004; Yang et al. 2019). Moreover, the origin and evolution of oceanic island arc rocks represent the clue for understanding how the continental crust was originated (Polat 2012). Accordingly, the oceanic island arc plutonic rocks (gabbroic rocks) of the Muiswirab area, Southeastern Eastern Desert, Egypt, gives an opportunity to detect the petrogenesis of the Neoproterozoic oceanic island arc plutonism, which contributed with the coeval volcanism in the evolution of Neoproterozoic continental crust.

The aim of this study is to present new major, trace, and rare earth element analyses and mineral composition data from samples of the Muiswirab metagabbros (MOM) in order to elucidate their petrogenesis and tectonic setting.

2 Previous work and geological setting

The Muiswirab area is situated immediately south the Migif-Hafafit domain and covers about 90 km^2 of basement crystalline rocks. The area is delineated by latitudes: 24°25′00″ and 24°28′53″N and longitudes: 34°37′07″ and 34°45′30″E (Fig. 1).

Although there are no previous studies concerned Muiswirab metagabbros and its granitoids or gave information about their petrological characteristic and tectonic evolution, but the metagabbros encountered in neighboring areas (e.g., Migif-Hafafit and Wadi El Gemal) have been best studied. On Hamata Quadrangle geological map (sheet NG36D, EGSMA 1997), prepared by the Egyptian Geological Survey and Mining Authority (EGSMA) in collaboration with the British Geological Survey (BGS), the MOM were mapped as late to post-tectonic mafic intrusion, whereas granitoids were identified as syn- to late-tectonic tonalite and granodiorite.

The investigated area represents a part of the so-called Wadi El Gemal-Hafafit terranes. Hegazy (1984), stated that the fine-grained hornblende gneisses represent most probably the lower part of the infrastructure in the Wadi El Gemal area, where the studied area is included. He added that the hornblende gneisses are bounded from the west and south by intrusive white gneissose granite and bounded from the east by massive and/or foliated metagabbros and the contact between them is marked by a zone of shearing. Moreover, he suggested that the Wadi El Gemal area

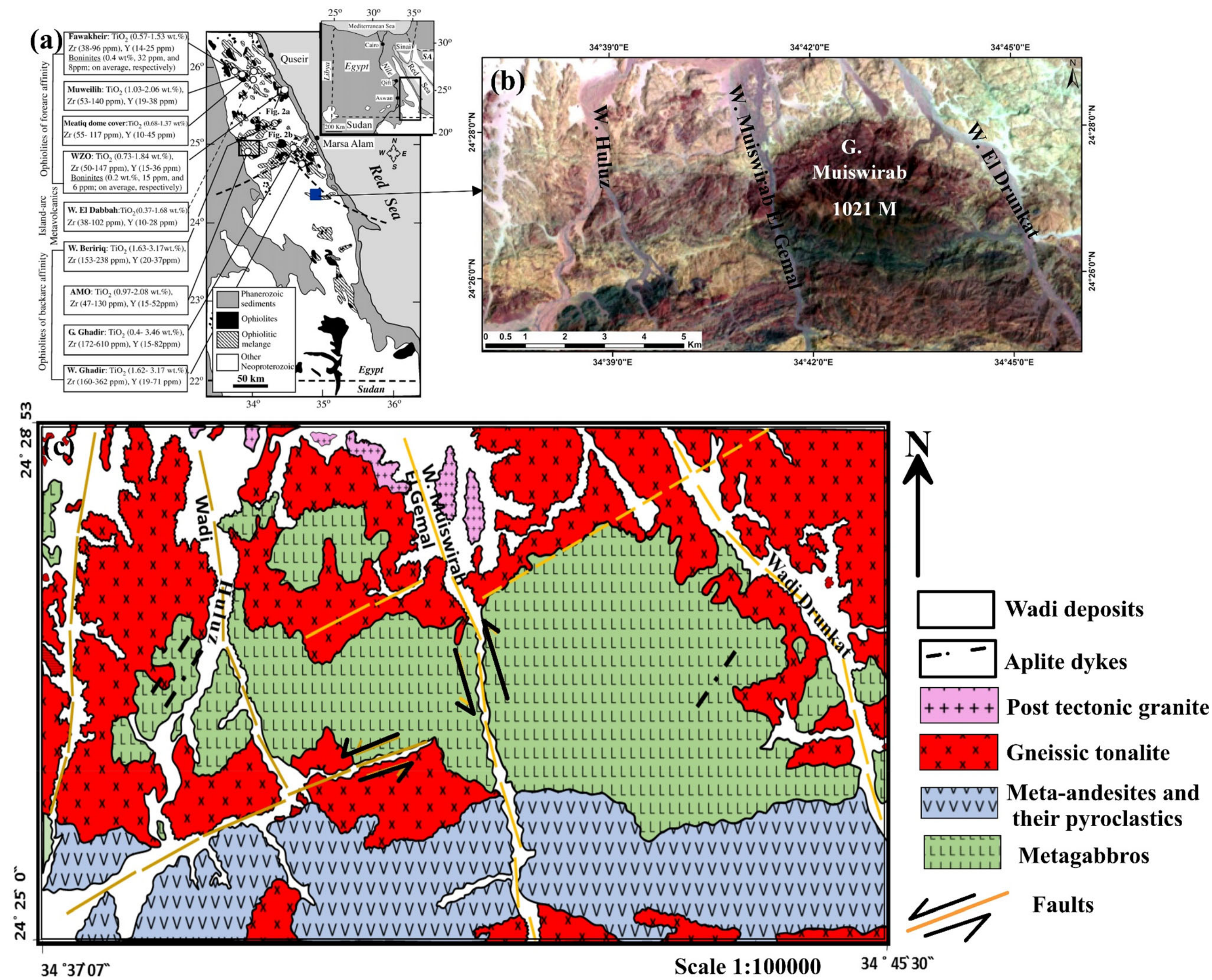

Fig. 1 **a** Distribution and ages of ophiolites and ophiolitic mélanges in the central (CED) and southern (SED) parts of the Eastern Desert of Egypt (after Farahat et al. 2004). The major shear zone (heavy dashed line) separating the CED and SED is from Stern and Hedge (1985), **b** Landsat image for the studied area, **c** simplified geologic map exhibiting the different rock units encountered in the investigated area

represents an old continental mass that has cratonized at least 1770 Ma ago and over which an oceanic crust has been abducted during the Pan-African orogeny. Rashwan (1991) mapped the so-called hornblende gneisses of Hegazy (1984) as metagabbros (mainly sub-alkaline) of medium grade metamorphism, and he added that some of these rocks are pertaining to intrusive island arc and others as regarded as remnants of an old oceanic crust. Ghoneim et al. (1992), arrive at the conclusion that the metagabbros (including MOM) which lies close to the eastern boundary of the Hafafit gneisses are composed of metagabbros, gneissose amphibolite, and subordinate diorite and, in general, have similarities with the ophiolitic gabbro. Stern and Hedge (1985), attempted dating of gneissic tonalite, which occupies the core of the northernmost dome of Migif-Hafafit area using combined Rb–Sr and U–Pb Zircon techniques. The two Zircon fractions studied gave an age of 682 Ma which interpreted as the time of emplacement and cooling of the plutons. Kröner et al. (1987), suggested that tonalitic plutons of the older granite suit south of Hafafit yielded U–Pb Zircons age of ≈ 710 Ma. In contrast, El Gaby et al. (1988, 1990) considered all the above granitoid gneisses as extensions of a Mid-Proterozoic crust exposed in the Western Desert of Egypt. In this view, the gneisses constitute a basement on to which the Pan-African supracrustal assemblage was deposited. Abu El Farh (2004) stated that the Hafafit granitoids range in composition from granodiorite through tonalite and trondhjemite, and are calc-alkaline, meta-aluminous, and pertaining to I-type granites and these rocks are believed to be of a volcanic-arc setting generated by subduction-related magmatism.

The Precambrian rocks of the Muiswirab area (Fig. 1c) are essentially a Pan-African assemblage comprising a metavolcanic group, mafic rocks (MOM), and granitoids. The metavolcanic succession is folded into a major asymmetrical syncline trending WNW–ESE. They are dissected by thrust faults, shear zones, and normal faults forming a graben that occurs in the southern parts beyond the map limits (Fig. 2) within which some sulfide mines are located. These metavolcanics are mafic (metabasalts) lavas and pyroclastic rocks (Helmy 1999). The mafic volcanic rocks cover about 30 km^2 and crop out as large belts extending nearly E–W, in the southern parts of the study area, and comprise massive and pillow lavas, lapilli, crystal tuffs, and agglomerates. Metabasalts are generally massive, amygdaloidal and occasionally pillowed. The metapyrocalstics occur as thinly laminated metatuffs (Fig. 2a).

The gabbroic rocks (MOM) of the study area are mainly represented by Gabal Muiswirab, which is located at the southeastern part of the mapped area (Fig. 2), and considered as the highest topographic feature herein. The elevation of the summit point of the mountain is 1021 M, and its top surface is discontinuous due to its interruption by NNW–SSE structural trend (Fig. 1c). Apart from the main mass small gabbroic bodies occur at the western and eastern sides of Wadi Huluz and Drunkat respectively (Fig. 1c). Other minor bodies from these rocks were encountered within the granitoids as big xenoliths. Based on the degree of deformation the gabbroic mass could be

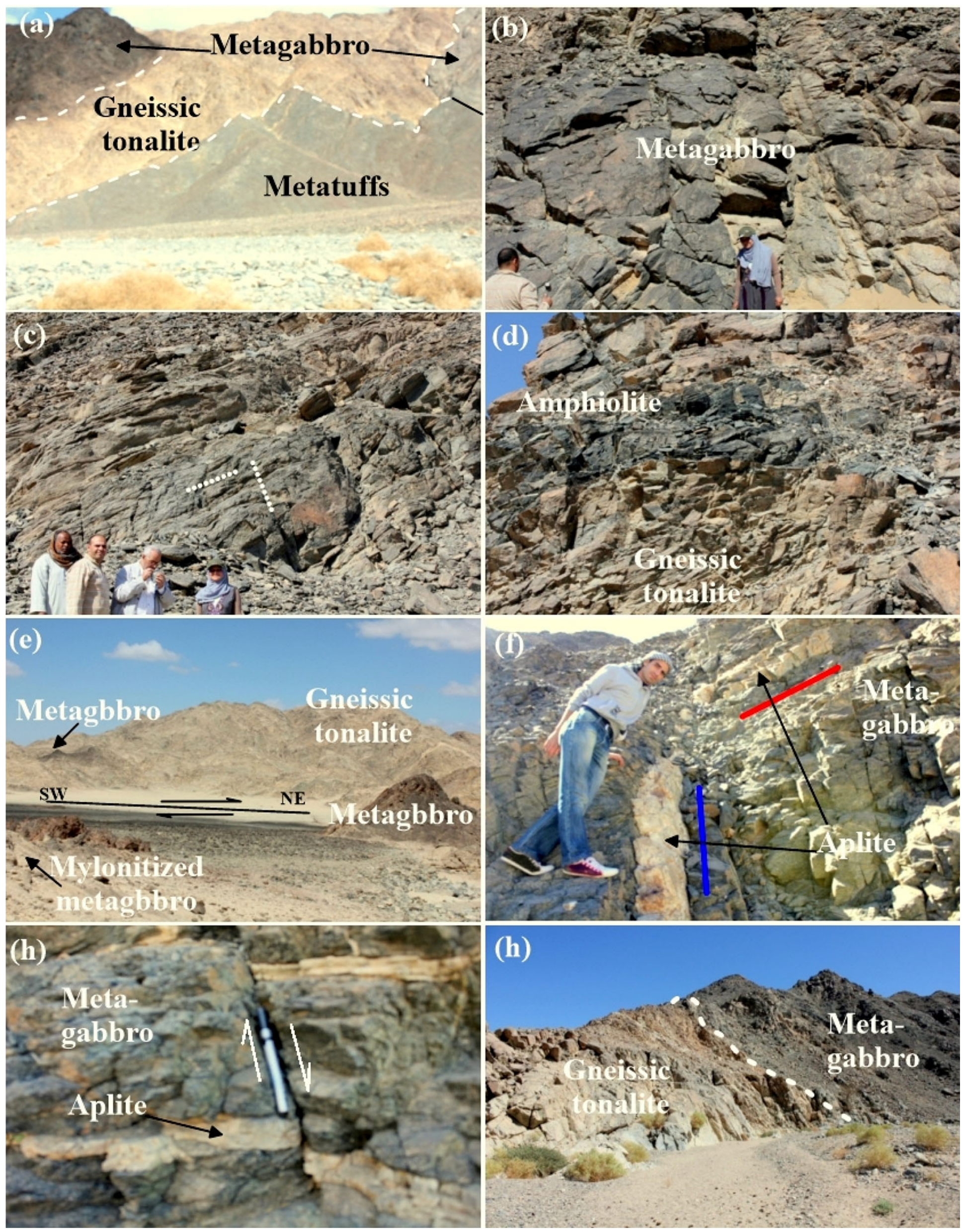

Fig. 2 Representative field photographs showing: **a** thin laminated metatuffs intruded by gneissic tonalite at the eastern flank of Wadi Drunkat, **b** close-up view showing cuboidal jointing of the massive metagabbros, **c** well developed flaser structure in the metagabbros of Wadi Huluz, **d** amphibolite lens intruded by gneissic tonalite at the western flank of Wadi Huluz, **e** fine-grained mylonite with finally crushed metagabbros, caused by fault trending NE–SW, **f** foliated metagabbros injected crosscut by two sets of aplite veins. The older is parallel to the old set of foliation, and the younger parallel to the second foliation of the host rock, **g** right lateral strike-slip fault running through the metagabbros and associated aplite vein at Wadi Huluz, **h** intrusive contact of the gneissic granitoids with the metagabbros, along Wadi Huluz

subdivided into two types. The first type (dominant) is massive and medium to coarse-grained (Fig. 2b) with hypidiomorphic granular texture and their mineralogical composition which is mainly plagioclase, pyroxene, and hornblende. In places, it is slightly foliated and metamorphosed. The second one (type) is represented by moderately to highly sheared metagabbros and consequently was subjected to more than one metamorphic episode, and was transformed into one of these constituents; uralitized gabbro, flaser gabbro, amphibolite, and protomylonite to mylonitized metagabbros (Fig. 2c–e). The gabbroic rocks are injected by a large number of aplite veins and lenticels either parallel to the flat-lying foliation or across it (Fig. 2f). Also, the aplite veins sometimes show weak foliation parallel to that of the enclosing rocks, and in few spots, they exhibit bending similar to recumbent folding. In addition, the aplite veins have been affected by right-lateral strike-slip fault (Fig. 2h). These features provide good evidence for the intense tectonic forces to which some parts of gabbroic rocks were subjected.

In general, the contacts of Muiswirab metagabbros with the metatuffs which exposed at the southern part of the map are sharp (Fig. 2a), whereas they intruded by the gneissic granitoids (Fig. 2h). Near this contact, the metagabbros become lighter in color due to the blastesis of feldspar, on the other hand, these rocks are intruded by small cupolas of pink granites.

The granitoids are exposed on the extreme western end of the Wadi El Gemal area and represent the NW extension of the huge batholith which lies southeast of the investigated area. Generally, these rocks occupied the northern part of the area under consideration, and cover an area about 48 km^2 (Fig. 1c). These rocks are generally foliated and forming isolated moderately hills and exhibit well-developed bouldery weathering and exfoliation. These rocks are clearly intruded into Muiswirab metagabbros (Fig. 2h), and in some places, they carry undigested blocks of these metagabbros (Fig. 2e). The enclosed lenticular bodies of metagabbros are conformable with the foliation of granitoids. In places, the contacts between the granitoids and the metagabbros are irregular and marked by interactions between both two rock units, producing zones of hybrid diorites. On the other hand, unmappable small outcrops of pink leucocratic granites are intruded within the granitoids. Generally, the gneissic granitoids in the peripheral zone of the exposure are strongly foliated, and sometimes they were transformed into protomylonite granitoids.

All the above-mentioned features provide good evidence for the intense tectonic forces to which these granites were subjected. From the foregoing, the numerous field evidence may indicate that these rocks are pertaining to the syn-tectonic granitoids and quite similar to the G1 granites of (Hussein et al. 1982).

3 Petrography

The following is a detailed petrographic description of the different rock units encountered in the investigated area with special emphasis on the gabbroic varieties.

3.1 The gabbroic rocks

As mentioned before these rocks represent the major rock unit of the area under consideration. Generally, the variation within these gabbroid rocks arisen chiefly from the change in the relative amounts of the alteration products i.e. (the secondary minerals) and the intensity of the deformation. Thus, they include four petrographic varieties, namely; metagabbros, uralitized gabbro, the flaser metagabbros and foliated amphibolite, and retrograde of amphibolitized gabbroic rocks.

The following is a detailed petrographic description of the different varieties of the studied metagabbros.

3.1.1 Metagabbros

These rocks are medium to coarse grained with a hypidiomorphic granular texture (Fig. 3a). They are composed mainly of calcic plagioclase ranging from bytownite to labradorite (An65-80), pyroxenes and little hornblende (Fig. 3b). Apatite, iron oxide are accessories and virtually free from olivine. Alteration products include saussurite, calcite, tremolite, actinolite, chlorite, and epidote, and exsolution lamellae between clinopyroxene and orthopyroxene grains are sometimes observed (Fig. 3b). These rocks exhibit ophitic, subophitic, and poikilitic textures (Fig. 3c). On the other hand, some samples exhibit cryptic layering with plagioclase rich layers alternating with mafic layers. Plagioclase is represented by bytownite to labradorite (An_{65-80}), which forms half the rock. It occurs as colorless, subhedral longitudinal crystals, and occasionally with tabular forms. In other samples, plagioclase is slight to moderately altered to aggregates of saussurite and epidote in the core and along the twin lamellae giving a cloudy appearance to the plagioclase. For fresh crystals still surviving, they show twinning according to albite, Carlsbad, and pericline laws. Some crystals are zoned; others show bent lamellae. In some samples, the plagioclase crystals either cracked and were filled by secondary calcite or corroded and replaced by epidote and calcite, as a result of deformation (Fig. 3d). Pyroxenes are represented by hypersthene and augite (Fig. 3c). Hornblende forms subhedral prismatic crystals and/or irregular patches. In some

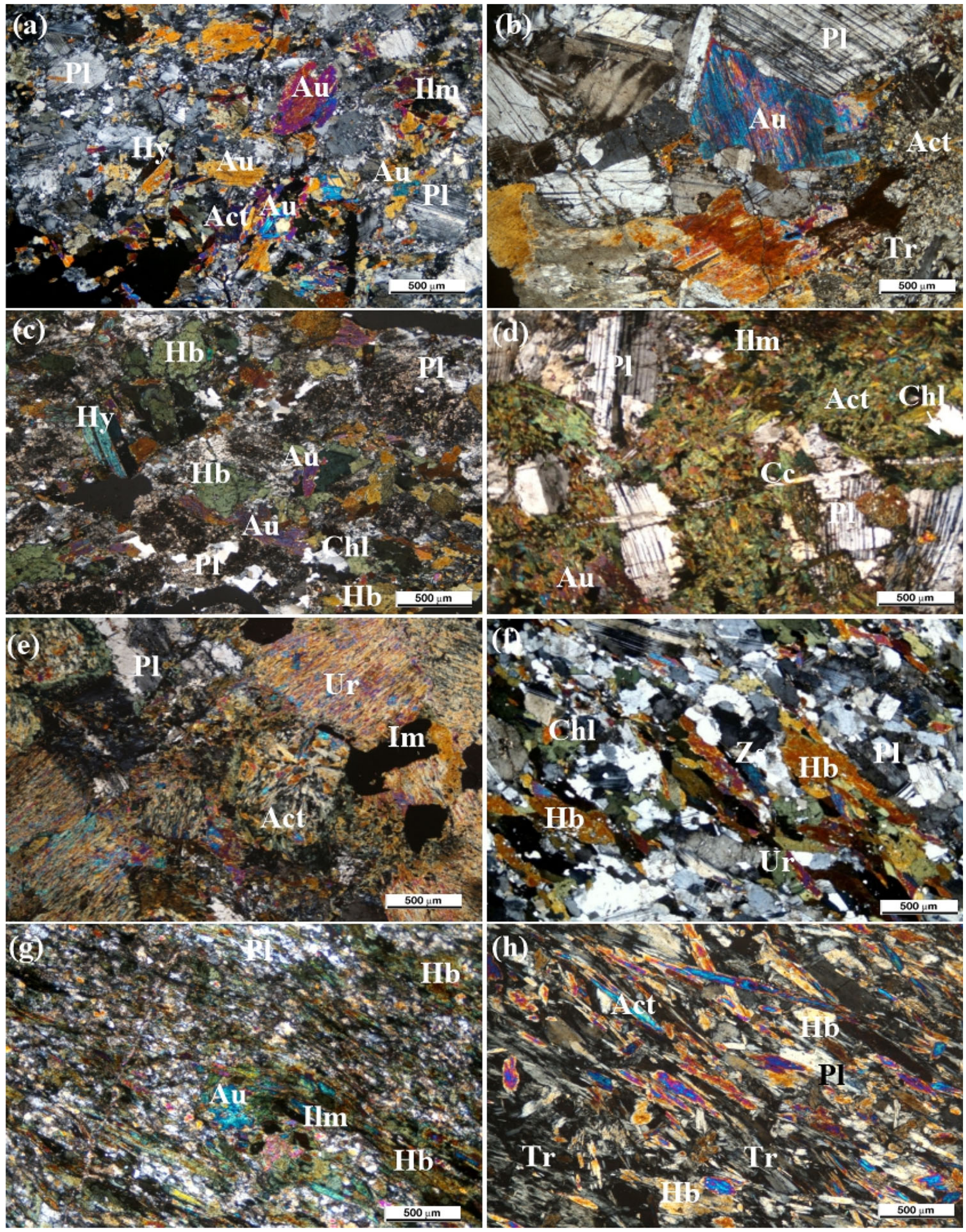

Fig. 3 Photomicrograph under cross nicols. **a** hypidiomorphic granular texture of metagabbros exhibiting replacement of augite to actinolite, **b** alteration products of metagabbros with exsolution lamellae of ortho- and clinopyroxene. *Note* clinopyroxene has been replaced marginally by amphibole, **c** highly altered metagabbros exhibiting ophitic and sub ophitic texture, **d** cracked plagioclase filled by secondary calcite, **e** uralitized gabbros exhibiting highly altered plagioclase, uralite and subordinate fibrous actinolite and opaques, **f** uralitized gabbros showing ink blue zoisite patches, **g** flaser metagabbros showing the well-developed orientation of amphibole minerals with remnants of augite, **h** foliated amphibolite showing well developed foliation represented by amphibole minerals. *Chl* chlorite, *Cc* calcite, *Hy* hypersthene, *Au* augite, *Ilm* ilmenite, *Zs* zoisite, *Hb* hornblende, *Act* actinolite, *Tre* tremolite, *Ur* uralite and *Pl* plagioclase

slices, hornblende occurs as aggregates and clots. It is of green color and is strongly pleochroic with pale green, green and dark green.

3.1.2 Uralitized gabbro

Uralitized gabbros are dominated in the western part of the outcrop. Microscopically, they are essential, composed of varying proportions of saussuritized calcic plagioclase (average An70); yellowish-brown secondary amphibole (uralite) with minor primary hornblende, and accessory actinolite, zoisite, magnetite, and remnant pyroxenes, crystals retained as tiny cores in the uralitic amphiboles (Fig. 3e). Some samples show parallel orientation of plagioclase crystals and uralite giving rise to a sort of cryptic layering (Fig. 3f). Uralite, are frequently seen as interlocking brown hornblende anhedral crystals with weakly pleochroic from yellowish-brown to brown (Fig. 3f). It forms a mantle around relics of pyroxene, and shows a schiller structure due to the presence of inclusions of iron rods arranged regularly parallel to the cleavage planes (Fig. 3e). Ink blue zoisite patches were observed in a few samples (Fig. 3f). Sometimes, hornblende occurs as a primary mineral encountered in a few thin sections associating uralite (Fig. 3f).

3.1.3 The flaser metagabbros and foliated amphibolite

3.1.3.1 The flaser metagabbros These rocks are dominantly exposed along the NE–SW fault planes which are parallel to the elongated side of the Gabal Muiswirab, thus they are characterized by a flaser structure. On the other hand, they are associated with the foliated amphibolite i.e. (intimately relationship). Generally, the flaser metagabbros are medium to coarse-grained with well-developed foliation and are greenish to reddish in color. Petrographically, they are mainly made up of plagioclase, hornblende, pyroxene, and relics of chlorite and actinolite, with well-developed flaser texture (Fig. 3g). Plagioclase, range in composition from bytownite to labradorite, it partly altered to saussurite. Hornblende crystals arranged in parallel alignment being occasionally curved around deformed plagioclase. Sometimes hornblende is replaced by chlorite. Few crystals of clinopyroxene occur as a prismatic shape with simple twinning and have faint pleochroism.

3.1.3.2 Foliated amphibolites These are dark green-colored, rather medium to coarse-grained rocks whose principle mineral components are hornblende and plagioclase, actinolite–tremolite, epidote, and chlorite are additional subordinate components (Fig. 3h). Generally, these rocks most probably derived from metagabbroic rocks, thus the plagioclase and hornblende tend to be equally abundant. These types of rocks show well developed foliated texture. Hornblende is the most dominant, it occurs as bluish-green to brownish-green in color, subhedral prismatic crystals or aggregates separated by plagioclase crystals. It is slightly altered to chlorite, epidote, and calcite. Plagioclase occurs as medium to coarse-grained plates or prisms with ragged edges either untwined or commonly showing lamellar and pericline twinning. It is labradorite to calcic andesine (Average An66) in composition. It is occasionally fractured and slightly altered to saussurite, some have bent twin lamellae.

4 Analytical techniques

The analysis of major element compositions of clinopyroxenes, secondary amphiboles, plagioclases, and chlorites were obtained in rock thin sections by electron microprobe analysis (EMPA) using a JEOL JXA8100 instrument with three wave spectrometers, completed with an INCA x-sight energy dispersive spectrometer at the Far Eastern Geologic Institute, Vladivostok of the Russian Academy of Sciences. The analytical conditions are 20 kV Accelerating voltage, beam current 15 nA and 10 to 30 s of counting time for silicate minerals. Raw data were revised by a PAP (Pouchou and Pichoir 1984) matrix correction. The oxides detection limits are 0.02 wt% for Si, Al, and K; 0.03 % for Ti, Mg, Ca, Ni, and Na, and 0.07 % for Fe, Cr and Mn. Representative EMPA data of minerals are given in the supplementary tables (S1, S2, S3 and S4).

A total of 19 representative gabbroic samples were analyzed for their major and trace elements contents at the Far Eastern Geologic Institute, Vladivostok of the Russian Academy of Sciences. The rock samples were crushed and then pulverized using an agate carbide ring grinder. Major oxides and selected trace element (e.g. V, Cr, Co, Ni, and Zn) analysis were carried out on powder pellets using an SRS 303 (Siemens) wavelength-dispersive XRF spectrometer operating at 50 kV and 50 mA. Loss on ignition (LOI) is calculated by the weight difference after ignition at 1000 °C. The accuracy was controlled by repeated measurements of standards and each sample was measured two times. Trace-element analyses including the rare earth elements (REE) by LA–ICP–MS (laser ablation–inductively coupled plasma–mass spectrometry) were carried out using an Agilent 7500 s quadrupole ICP–MS system attached to a New Wave/Merchantek UP213 laser ablation system. Detection limits range from 0.003 to 0.03 wt% for major oxides, 0.1 to 30 ppm for trace elements and 0.03 to 0.1 ppm for the REEs. Whole-rock major and trace element data are reported in the supplementary table S5.

5 Mineral chemistry

The microprobe analyses for major elements together with the recalculated cations of the clinopyroxene, amphibole plagioclase, and chlorite in the investigated metagabbros are listed on supplementary tables (S1-S4).

5.1 Clinopyroxenes

The analyzed clinopyroxenes (Cpxs) from the MOM rocks are Mg-rich with Mg# ranging from 0.71 to 0.82 (Table S1) and exhibiting a wide range in composition (En39–48 Fs13–17 Wo36–46). Meanwhile, they exhibit a wide variation of both TiO_2 and Al_2O_3 (0.01–0.49 and 0.75–2.81, respectively. The analyzed clinopyroxenes are mainly of augite composition, together with the subordinate diopside and show a trend toward increasing Mg and decreasing Ca contents (Fig. 4a). All the analyzed clinopyroxenes plot in the subalkaline field (including MORB; Fig. 4b), pointing to the ophiolitic affinity of the investigated gabbroic rocks. In addition, the relatively low abundance of Ti in the analyzed clinopyrocenes point to the tholeiitic affinity (Leterrier et al. 1982) of the MOM rocks. For further confirmation of the ophiolitic affinity of the studied rocks; most of the analyzed clinopyroxenes plot in the field of orogenic tholeiitic basalts particularly of boninitic compositions (Fig. 4c). Moreover, Loucks (1990) stated that the Al/Ti in clinopyroxene from mafic and ultramafic rocks could be used to point out whether they are related to ophiolitic or non-ophiolitic rocks. Accordingly, the variation trend of the analyzed clinopyroxene coincides with the trend of Bay of Islands ophiolite (Fig. 4d).

5.2 Amphiboles

Generally, the MOM rocks have higher contents of amphiboles. The chemical composition of the analyzed amphiboles are given in supplementary Table S2. Based on the classification of Hawthorne et al. (2012), they are secondary calcic amphiboles. The analyzed amphiboles show a general increase of their Na and K contents with an

Fig. 5 **a** Plot of $Al^{(iv)}$–(Na + K) in A-site for amphiboles in the studied metagabbros. Nomenclature from Hawthorne et al. (2012). **b** Plots of Ti–(Na + K) in B-site for distinction between igneous and metamorphic amphiboles (Girardeau and Mevel 1982) in the studied metagabbros. **c** Classification diagram for plagioclase feldspars from the studied metagabbros, compositional fields are after Deer et al. (1992), **d** Chlorite classification system of showing the composition of chlorite from the studied gabbroic rocks, **e** Plots of Mg#–Al^{iv} for chlorite from the studied metagabbroric rocks, **f** Al–Fe–Mg diagram exhibiting the composition of the studied chlorites; field of greenschist facies chlorite after Velde and Rumble (1977) ▶

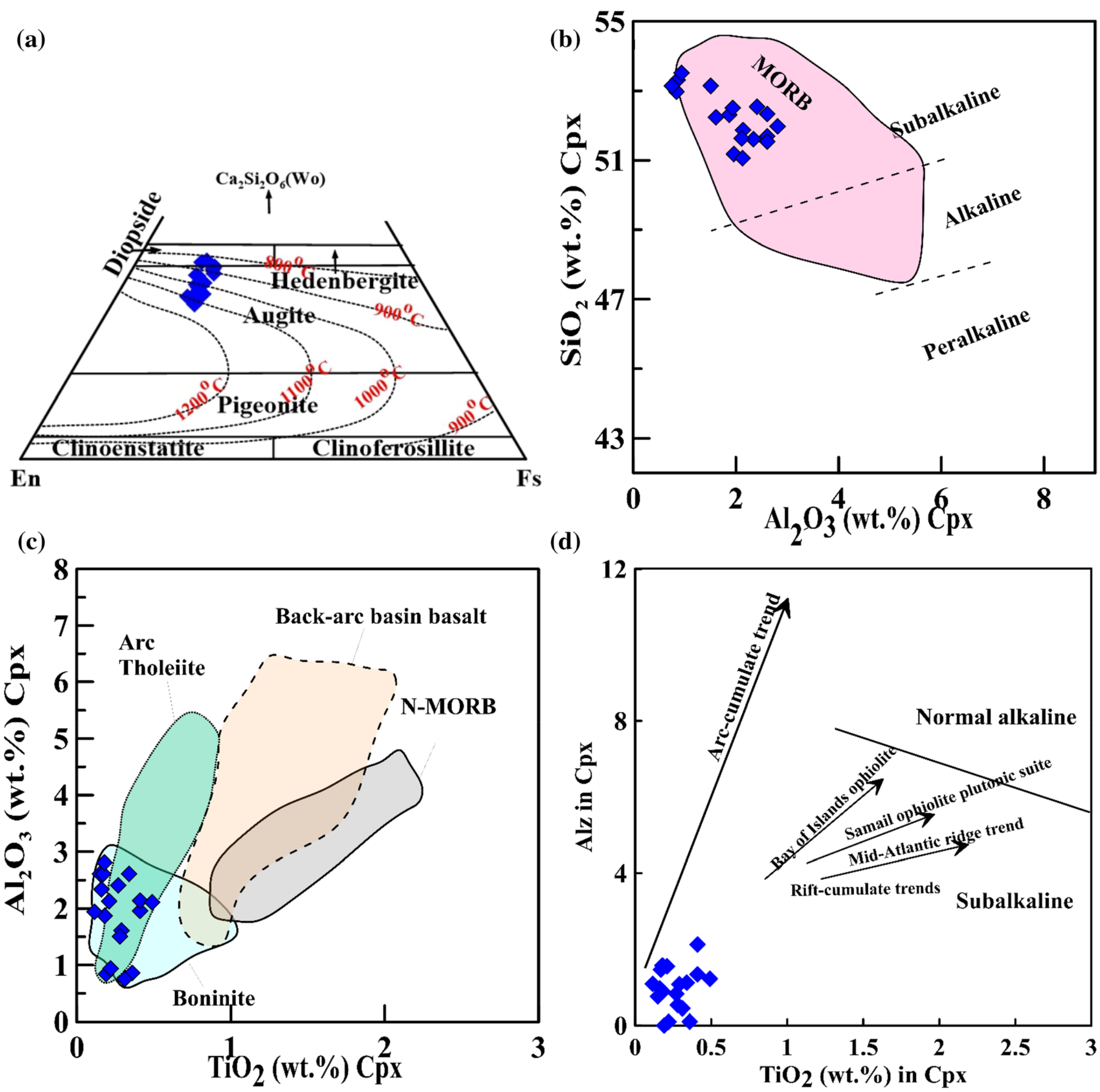

Fig. 4 Classification and tectonic discrimination diagrams based on clinopyroxene mineral chemistry of the studied metagabbros. **a** Classification and compositional variation diagram after Morimoto et al. (1988); isotherm curves of a two pyroxene geothermometers after Lindsley (1983), **b** SiO_2–Al_2O_3 diagram of Le Bas (1962) for clinopyroxene. Field of mid ocean ridge basalt (MORB) is from Nisbet and Pearce (1977), Manya (2014), **c** Al_2O_3–TiO_2 adapted after Huot et al. (2002), **d** Alz (Al^{iv}*100/2)–TiO_2 diagram; the trends arrow of different tectonic settings are obtained from Loucks (1990). Symbol in Figs. 4, 5, 6, 7, 8, 9, 10, 11, 12: ◆ studied metagabbros

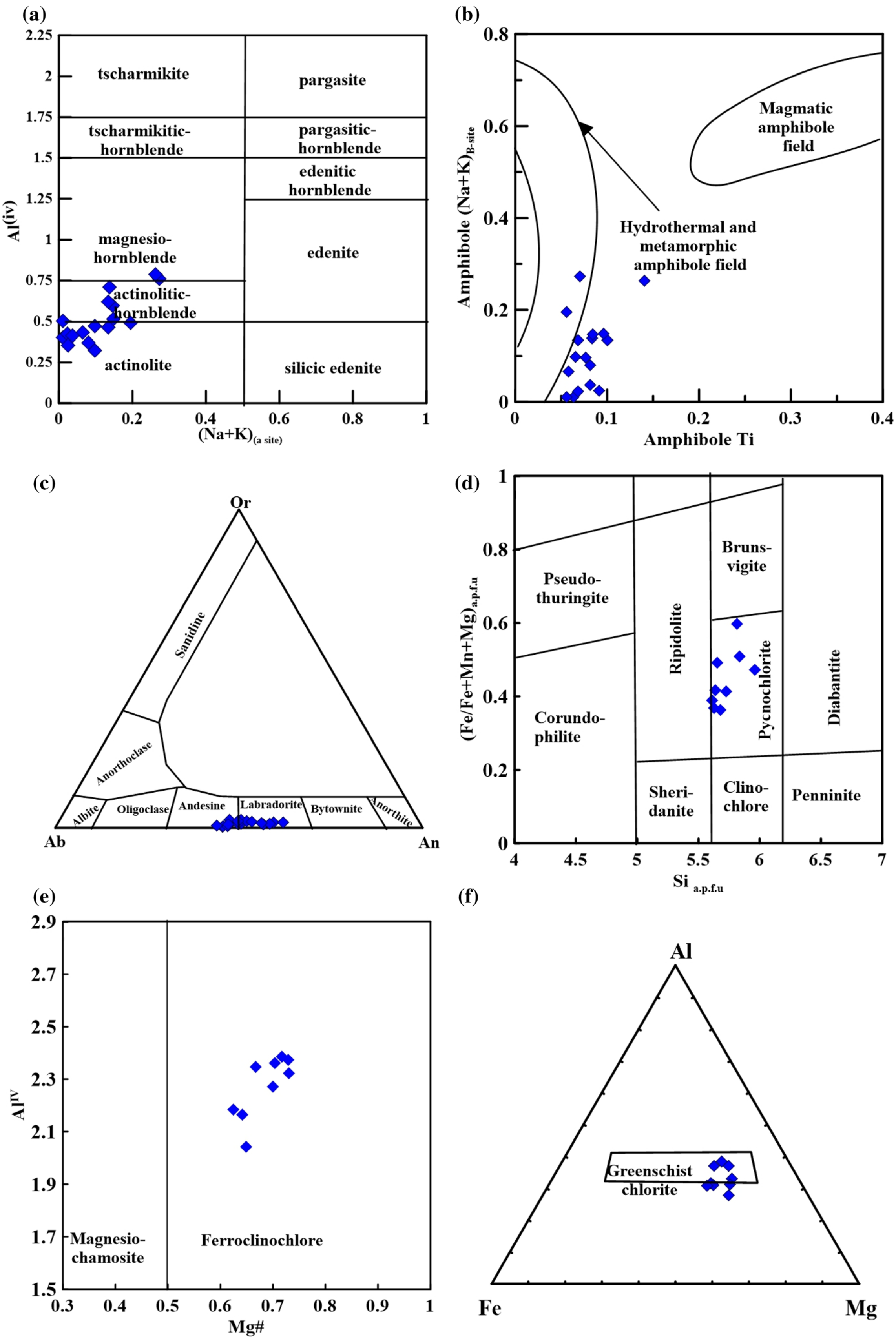
(a)
tscharmikite
pargasite
tscharmikitic-hornblende
pargasitic-hornblende
edenitic hornblende
magnesio-hornblende
edenite
actinolitic-hornblende
actinolite
silicic edenite
Al(iv)
(Na+K)(a site)
(b)
Magmatic amphibole field
Hydrothermal and metamorphic amphibole field
Amphibole (Na+K)B-site
Amphibole Ti
(c)
Or
Sanidine
Anorthoclase
Albite
Oligoclase
Andesine
Labradorite
Bytownite
Anorthite
Ab
An
(d)
Pseudo-thuringite
Ripidolite
Bruns-vigite
Pycnochlorite
Diabantite
Corundo-philite
Sheri-danite
Clino-chlore
Penninite
(Fe/Fe+Mn+Mg)a.p.f.u
Si a.p.f.u
(e)
Magnesio-chamosite
Ferroclinochlore
Al^{IV}
Mg#
(f)
Al
Greenschist chlorite
Fe
Mg

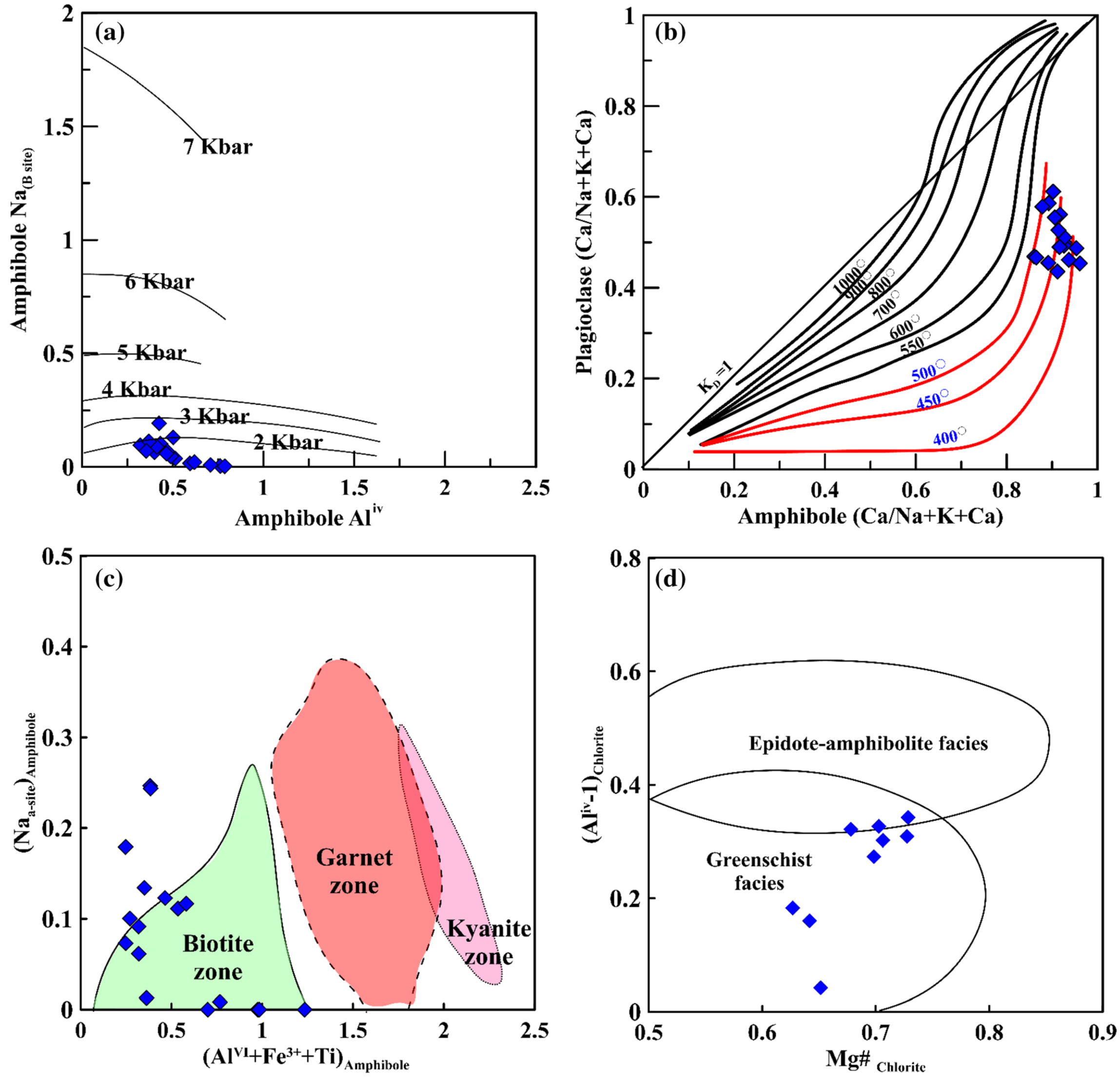

Fig. 6 **a** Plot of Al^{iv}–Na cation in B-site of the studied amphiboles. Pressure curves after Brown (1977), **b** plot of studied amphibole-plagioclase pairs in the distribution diagram given by Perchuk (1970) cited in Ulrych et al. (1976), **c** plot of amphiboles formula proportion variation diagrams of the studied amphiboles in relation to Laird and Albee (1981) defined zones, **d** plot of Al^{iv}–Mg# of the studied chlorite. Fields of metamorphic facies conditions of regional metamorphism after Bailey (1988)

increase of their Al contents (Fig. 5a). They are essentially actinolite with subordinate actinolitic hornblende and extending into the field of magnesio-hornblende (Fig. 5a). The Mg# increase from actinolite through actinolite hornblende to the magnesio-hornblende (Table S2). The analyzed amphiboles possess relatively high Al_2O_3 contents, particularly in actinolite (up to 9.65 wt%) in contrast to actinolitic hornblende (up to 6.13 wt%) and magnesio-hornblende (up to 6.44 wt%) (Table S2). Girardeau and Mevel (1982), used the alkali (Na + K)/Ti ratio to distinguish between the metamorphic and igneous amphiboles. Accordingly, the analyzed amphiboles are related to metamorphic amphiboles as they plots within or close to the field of metamorphic amphiboles (Fig. 5b). The magnesio-hornblende and actinolite might have been formed as secondary hornblendes by reaction of the earlier pyroxene with the increasingly water-rich magma. The Mg# of the analyzed amphibole samples range from 0.63 to 0.78, which are generally lower than the Mg# of the analyzed clinopyroxenes from the same samples suggesting that these amphiboles are most likely represents late metamorphic minerals rather than reflecting later magmatic crystallization (Singh et al. 2016).

5.3 Plagioclase

Representative EMP analyses of plagioclase from the MOM rocks are listed in supplementary table S3.

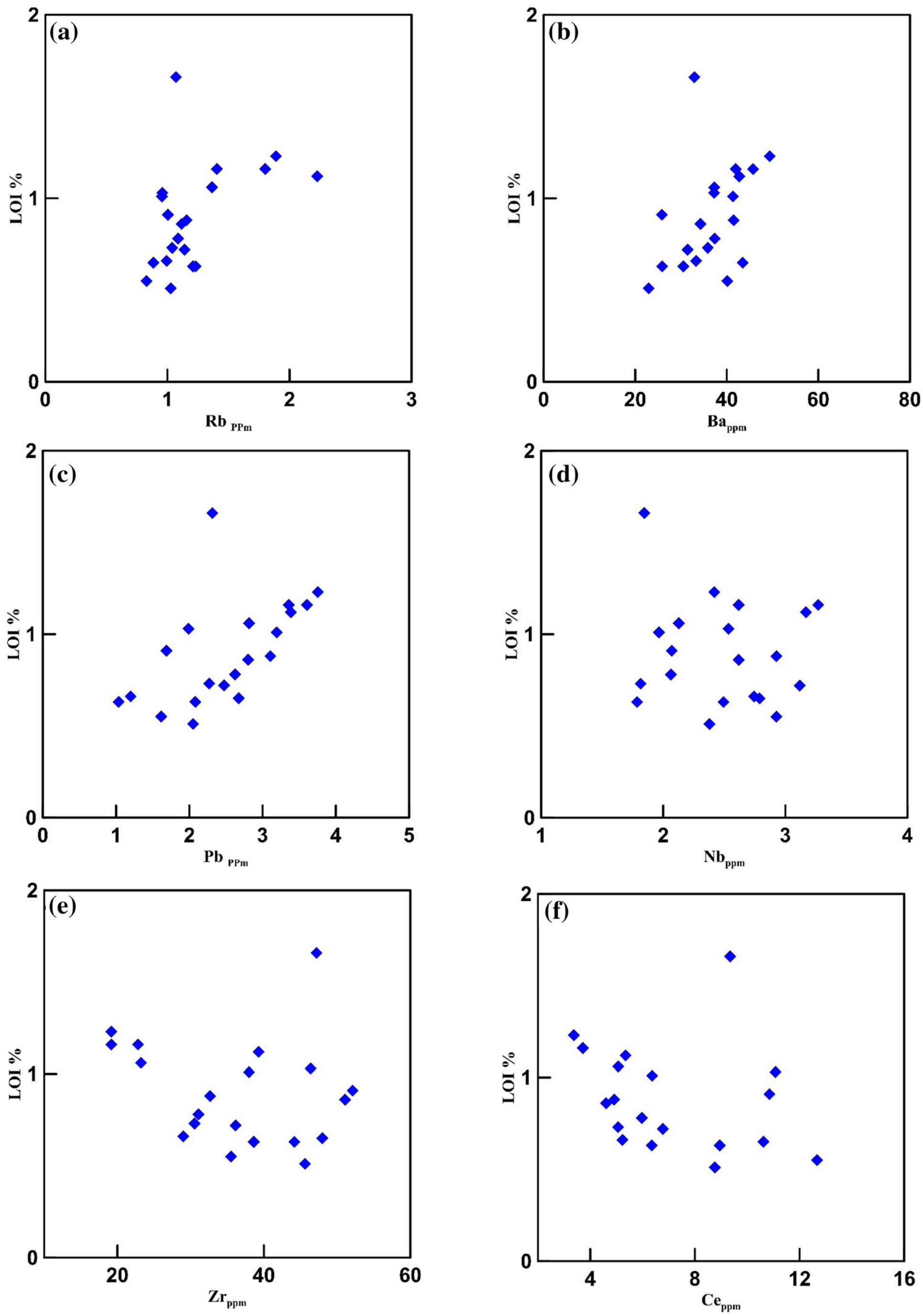

Fig. 7 Variation of loss on ignition (LOI) versus fluid–mobile and fluid–immobile elements showing a LOI. **a–c** Showing the positive correlation between LOI and Rb, Ba and Sr, respectively. **d–f** Exhibiting no distinct correlation between LOI and Nb, Zr and Ce, respectively

Generally, the analyzed plagioclase are homogeneous in composition and possess high contents of CaO (9.11–12.47 wt%) and Al_2O_3 (25.01–30.22 wt%) with low contents of TiO_2, Na_2O and K_2O (Table S3). They are sodic enriched and have a wide variation of anorthite contents ($An_{43.57–60.14}$) and ranging in composition from labradorite to andesine. The wide range of An contents reflects the presence of An-rich plagioclase relics as well as metamorphic plagioclase (andesine; Fig. 5c).

5.4 Chlorite

Chlorites from the investigated MOM rocks are relatively Mg-rich and classify as pycnochlorite and ripidolite and

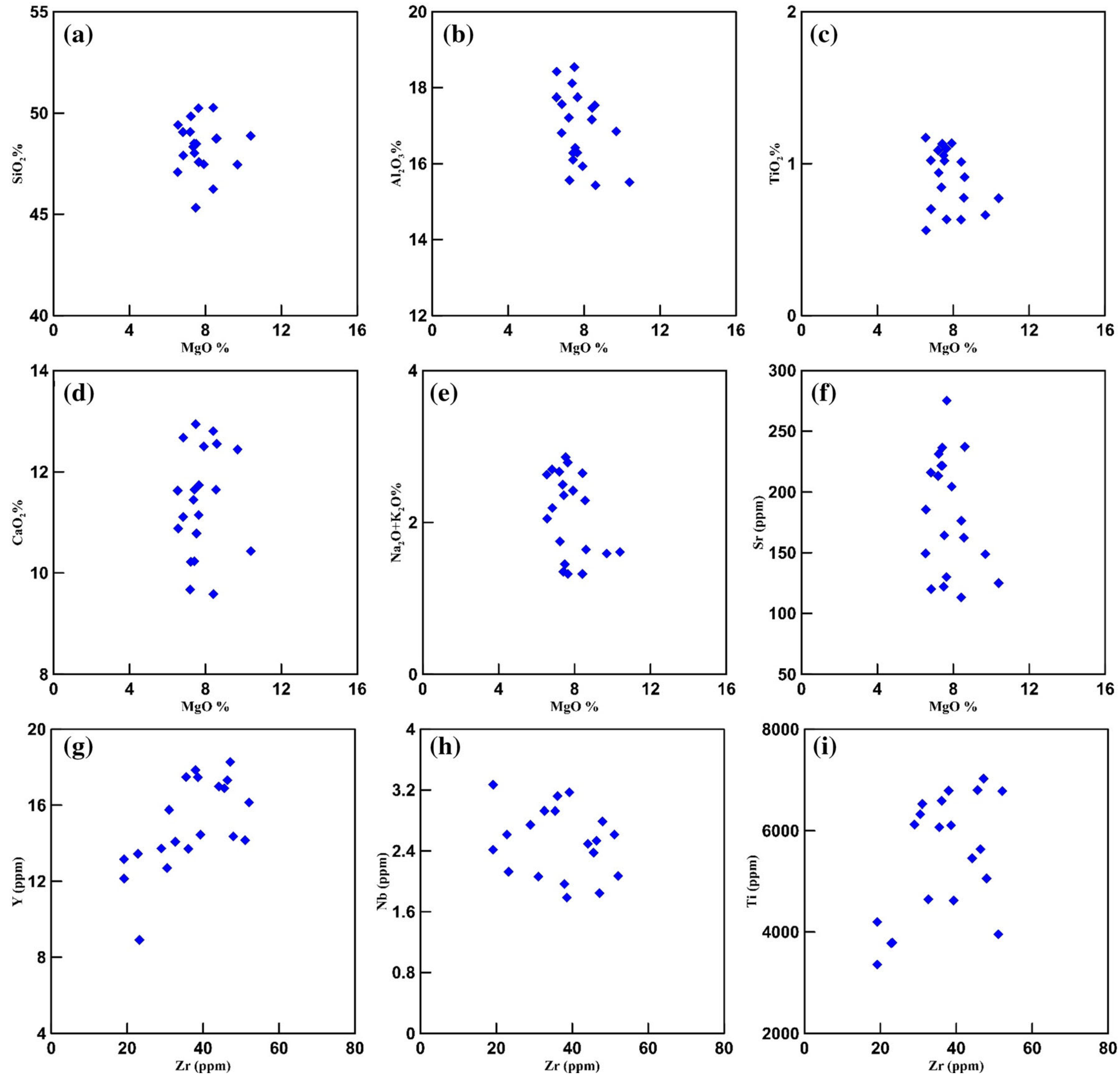

Fig. 8 Selected major and trace elements concentrations of the investigated metagabbros plotted against MgO (**a**–**f**) and Zr (**g**–**i**)

have higher Mg-numbers (Fig. 5d, e). Their Si concentrations range between 5.38 and 5.78 a.p.f.u. (based on 22 oxygens; Table S4) whereas Fe/(Fe + Mg + Mn) ratios ranges from 0.20 to 0.34. Generally, the analyzed chlorites plots within or close to the field of the greenschist facies (Fig. 5f) and most probably reflect retrogression (Winkler 2013).

6 Metamorphic conditions of the studied gabbroic rocks

The metamorphic conditions of MOM rocks could be assigned using their minerals chemical compositions. The principle of the clinopyroxene thermometer of Lindsley (1983) is based mainly on the partitioning of Ca between coexisting low-Ca and high-Ca pyroxenes since there is a strong temperature dependence of Ca-exchange between both. With decreasing temperature Ca increases in high-Ca pyroxenes and decreases in low-Ca pyroxenes at a given Mg/Fe ratio for the pyroxenes (Lindsley 1983). In the analyzed clinopyroxene samples, the same behavior is observed, the major trends show that the Ca-content mainly increases in augite. The highest crystallization temperature (up to > 1100 °C) is obtained by the few Mg-rich augite while the lowest temperature (up to 850 °C) is obtained by the Ca-rich augite (Fig. 4a).

Mineral assemblage observed in the MOM rocks suggesting regional metamorphism, which evidenced by the replacement of the primary clinopyroxene and plagioclase (Fig. 3a). Although MOM rocks retain some relict igneous textural and mineralogical features, their pyroxenes are

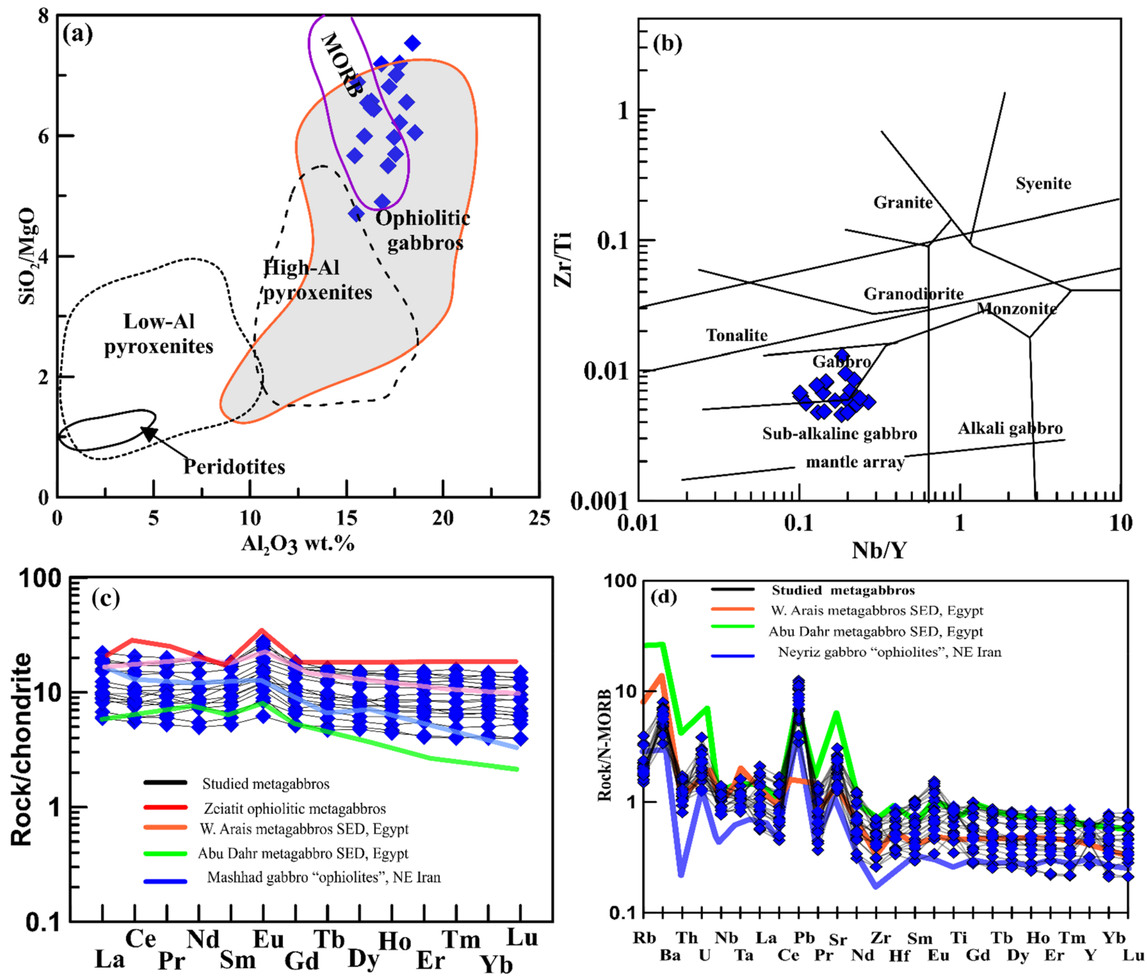

Fig. 9 **a** Al_2O_3–SiO_2/MgO diagram (Bodinier and Godard 2003) for the studied metagabbros, **b** plots of the studied gabbroic rocks on the rock classification diagram based on the Zr/Ti–Nb/Y ratios (Winchester and Floyd 1977), **c** chondrite normalized REE pattern for the studied metagabbros, **d** N-MORB normalized multi element plots for the studied metagabbros. For **c** and **d** normalizing values are from Sun and McDonough (1989). The representative samples of Egyptian metagabbros; of Abu Dahr, Wadi Arais and Zeiatit metagabbros and Neyriz metagabbros from Iran are after Gahlan et al. (2015), Obeid et al. (2016), Mogahed (2019) and Moghadam et al. (2014) respectively are plotted for comparison

generally replaced by secondary minerals (e.g., actinolitic hornblende, chlorite and epidote), whereas plagioclase is generally saussuritized. The petrographic investigation of the investigated gabbroic rocks indicates that they have metamorphic minerals including actinolite, albite, chlorite, and epidote which are typical for the greenschist facies. The analyzed amphiboles are mainly related to metamorphic amphiboles (Fig. 5a, b). In addition, based on their chemical composition (Table S2), these amphiboles seem to be formed mainly at low-pressure of about 1–3 kbar (Fig. 6a) and at a temperature range of 450 to 500 °C (Fig. 6b). Moreover, the analyzed amphiboles plot within or close to the biotite zone (Fig. 6c), which pertains to the greenschist facies metamorphism (350–500 °C and < 6 kbar; Liou et al. 1985). The results of the various amphibole geobarometers of MOM are listed in Table 1. Based on the barometric calculations of Ridolfi et al. (2010), the analyzed amphiboles exhibiting pressure ranging from 0.8 to 2.8 kbar with an average of 1.8 kbar.

The chemistry of chlorite from the MOM rocks can be used to calculate temperature of regional metamorphism and metamorphic grade. Generally, the chlorite minerals are sensitive to variation in temperature related to the common substitutions and occupancies of Fe, Mg, and Al in both tetrahedral and octahedral sites (Jiang et al. 1994; Inoue et al. 2009, 2010). The analyzed chlorites from the investigated MOM are mainly pycnochlorite (Fig. 5d) and seem to be formed at the conditions of the upper greenschist facies condition (Fig. 6c, d). In addition, the chemistry of chlorite could be used as a geothermometer (Cathelineau and Nieva 1985) on the basis of Al cations and Fe/Fe + Mg ratio. Applying this geothermometer on

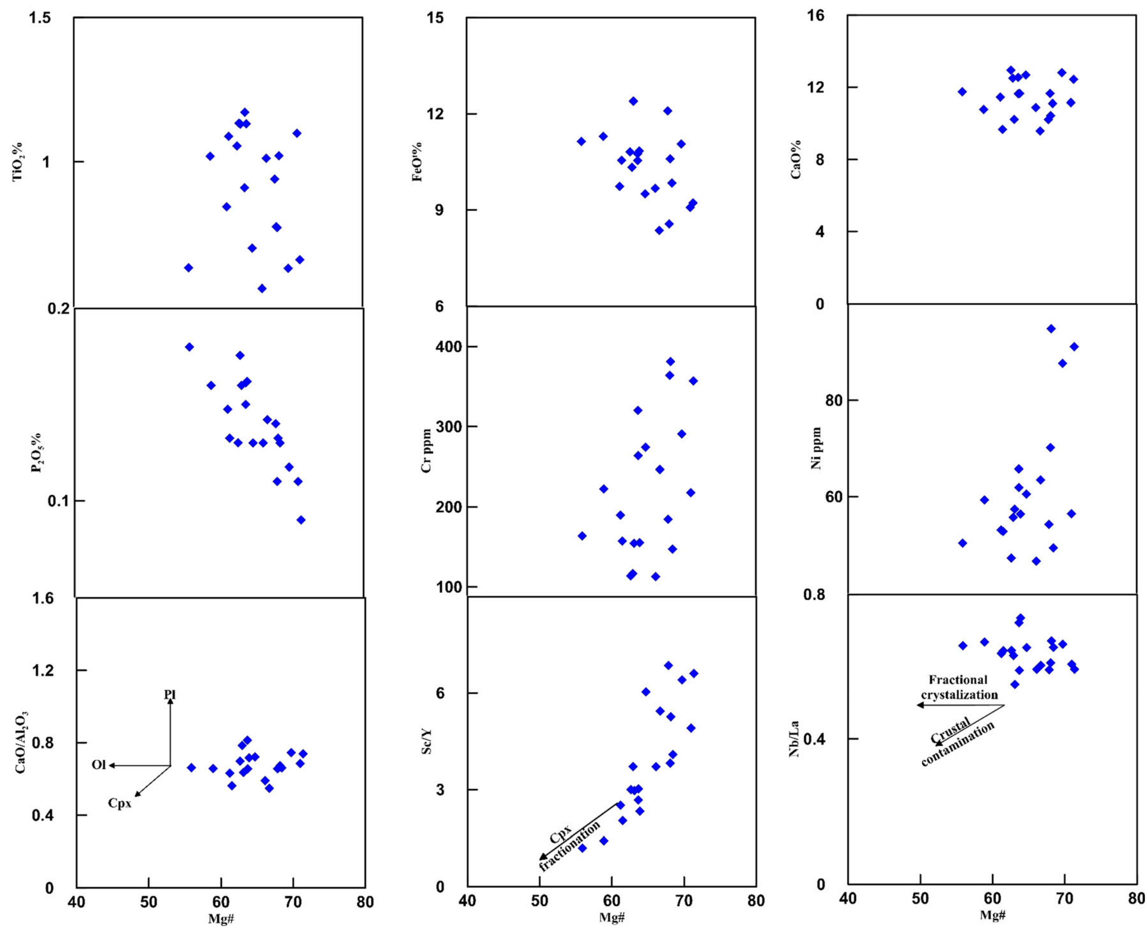

Fig. 10 Plots of TiO_2, FeO^t, CaO, P_2O_5, Cr, Ni, CaO/Al_2O_3, Sc/Y and Nb/La versus Mg# for the studied metagabbros

the analyzed chlorite yields estimated temperature ranging from 265 to 292 °C. This geothermometer adopted for chlorite with (Fe/Fe + Mg) ranging 0.18–0.64 (Cathelineau and Nieva 1985) which are appropriate for the studied samples. The temperatures obtained suggest the formation of chlorite at the expense of calcic amphibole as a retrograde phase typical of greenschist facies conditions (Bailey 1988).

7 Whole-rock geochemistry of the studied gabbroic rocks

Whole-rock major oxide, trace elements, and rare earth elements (REE) data for 19 representative samples from MOM are presented in the supplementary Table S5. The analyzed rock samples have SiO_2 ranging between (45.32–50.27 wt%), these rocks are characterized by moderate to high Al_2O_3 (15.43–18.54 wt%), high MgO (6.54–10.39 wt%), CaO (9.58–12.94 wt%), and FeO^t (8.36–12.93 wt%), and have low K_2O (0.10–0.41 wt%). Moreover, MOM have low TiO_2 (0.56–1.17 wt%), P2O5 (0.10–0.18 wt%), Zr (37.51–69.50 ppm), Nb (generally < 3 ppm), Y (8.92–18.27 ppm), and Ba/Zr (0.33–1.23). Although field and petrographic observations indicated that the MOM have undergone some degree of alteration and metamorphism but their chemical compositions exhibit low values of loss on ignition (LOI; 0.51–1.66; Table S5). In addition, the concentrations of fluid-mobile elements such as Rb, Ba, and Pb are positively correlated with LOI (Table S5 and Fig. 7), and thus, we suggest that these elements have been enriched by hydrothermal alteration. On the other hand, the fluid-immobile incompatible trace elements Ti, Nb, Zr, and the REE (Table S5 and Fig. 7) show systematic variations with LOI indicating that the concentrations of such elements did not significantly change by the hydrothermal alteration processes. Moreover, the very low concentrations of $Na_2O + K_2O$ contents (1.32–2.86 wt%; Table S5) indicate the cumulate nature of the rocks. This cumulate nature is evidenced by the variation diagrams of MgO against some major elements (Fig. 8). The sample plots of the investigated gabbroic rocks occur as clusters with a limited degree of scattering (Fig. 8) reflecting their cumulative nature.

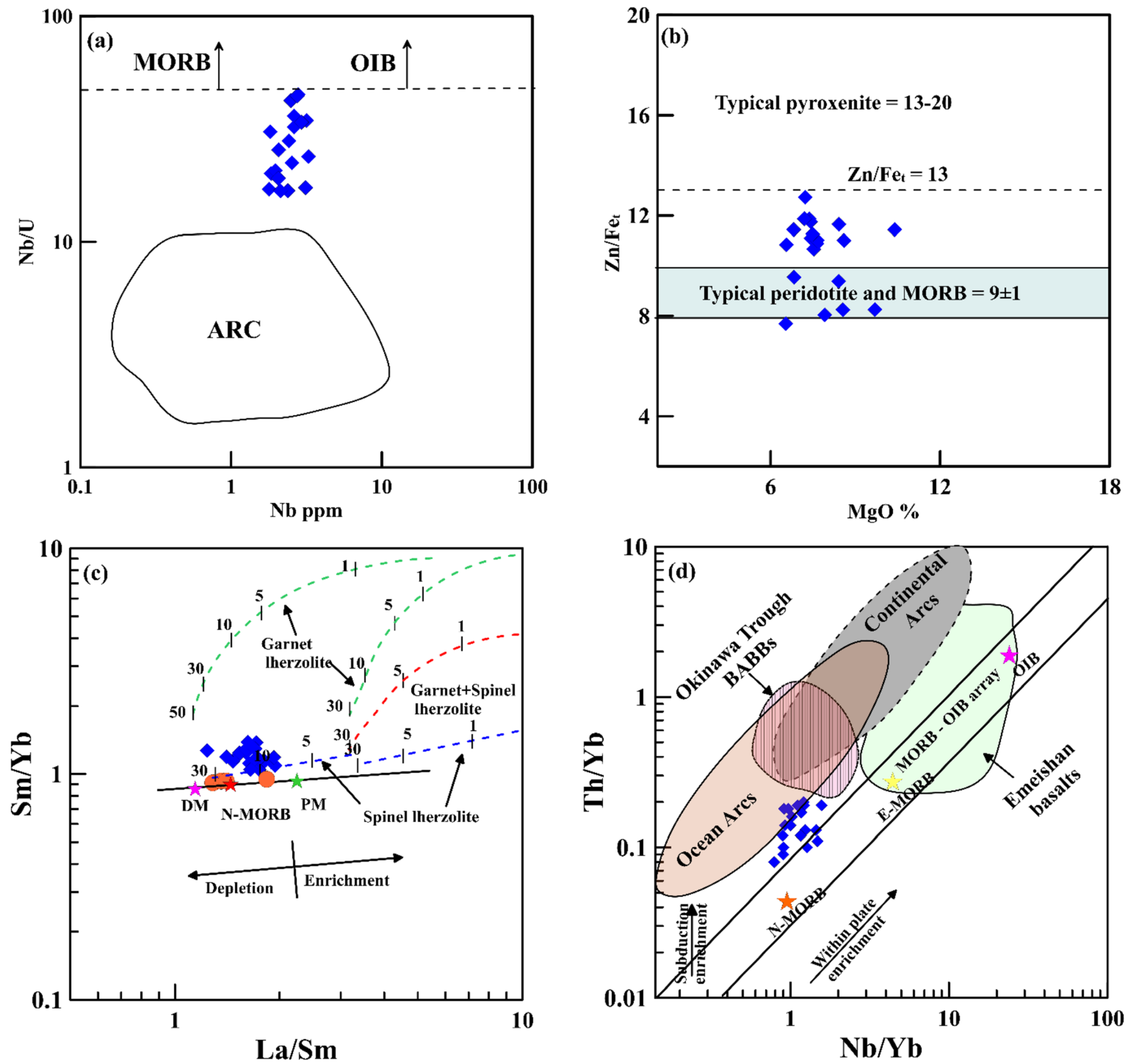

Fig. 11 **a** Nb/U versus Nb diagrams for the studied MOM rocks. Data sources: ARC, MORB and OIB are after O'Neill and Jenner (2012), **b** Zn/Fe^t ($\times$ 10^4) versus MgO for the studied MOM rocks. Peridotite and pyroxenite fields based on the Zn/Fe^t ratio are after Le Roux et al. (2010, 2011), Murray et al. (2015), **c** Sm/Yb–La/Sm diagram for studied metagabbros. Melting curves are after Bezard et al. (2011); symbols represent data obtained from the Egyptian ophiolitic metagabbros of Wadi Arais area (Obeid et al. 2016), Abu Dahr (Gahlan et al. 2015), Fawakhir area (Abd El-Rahman et al. 2009) and Zeiatit area (Mogahed 2019) are shown for comparison, **d** Th/Yb–Nb/Yb diagram for the studied metagabbros. Discrimination fields of oceanic arcs, continental arcs and MORB–OIB mantle array are from Pearce (2008, 2014), field of Okinawa Trough BABBs after Shinjo et al. (1999) and field of Emeishan basalts after Xu et al. (2001), Xiao et al. (2004), He et al. (2010)

Furthermore, Al_2O_3 and Sr exhibiting weakly negative correlation with MgO (Fig. 8b, f) indicates that the plagioclase did not crystallize during the fractional crystallization process and thus increased modally at the end of the process. However, the negative correlation between MgO and Al_2O_3 indicates that pyroxene and possibly olivine took part in early crystallization (Kocak et al. 2005). Moreover, the plots of Zr against some of high field strength elements (HFSE) such as Y, Nb, and Ti (Fig. 8g, h) exhibit a linear relationship with some degree of scattering suggesting that all the gabbroic rocks are probably formed from a single parental magma and indicate that the HFS elements rather less affected by secondary alteration processes (Staudigel 2003).

The investigated MOM exhibiting subalkaline characters as they plot within the subalkaline fields on the total alkali versus silica (TAS) diagram (Cox et al. 1979). Moreover, they plot in the tholeiitic gabbro field (supplementary figure S1a). Chemically, the MOM rocks are classified as ophiolitic rocks based on the Al_2O_3 versus SiO_2/MgO diagram (Fig. 9a) of Bodinier and Godard (2003). As the invesigated mafic rocks have suffered from at least greenschist facies metamorphism (Figs. 3, 5), thus the remobilization of elements should be considered.

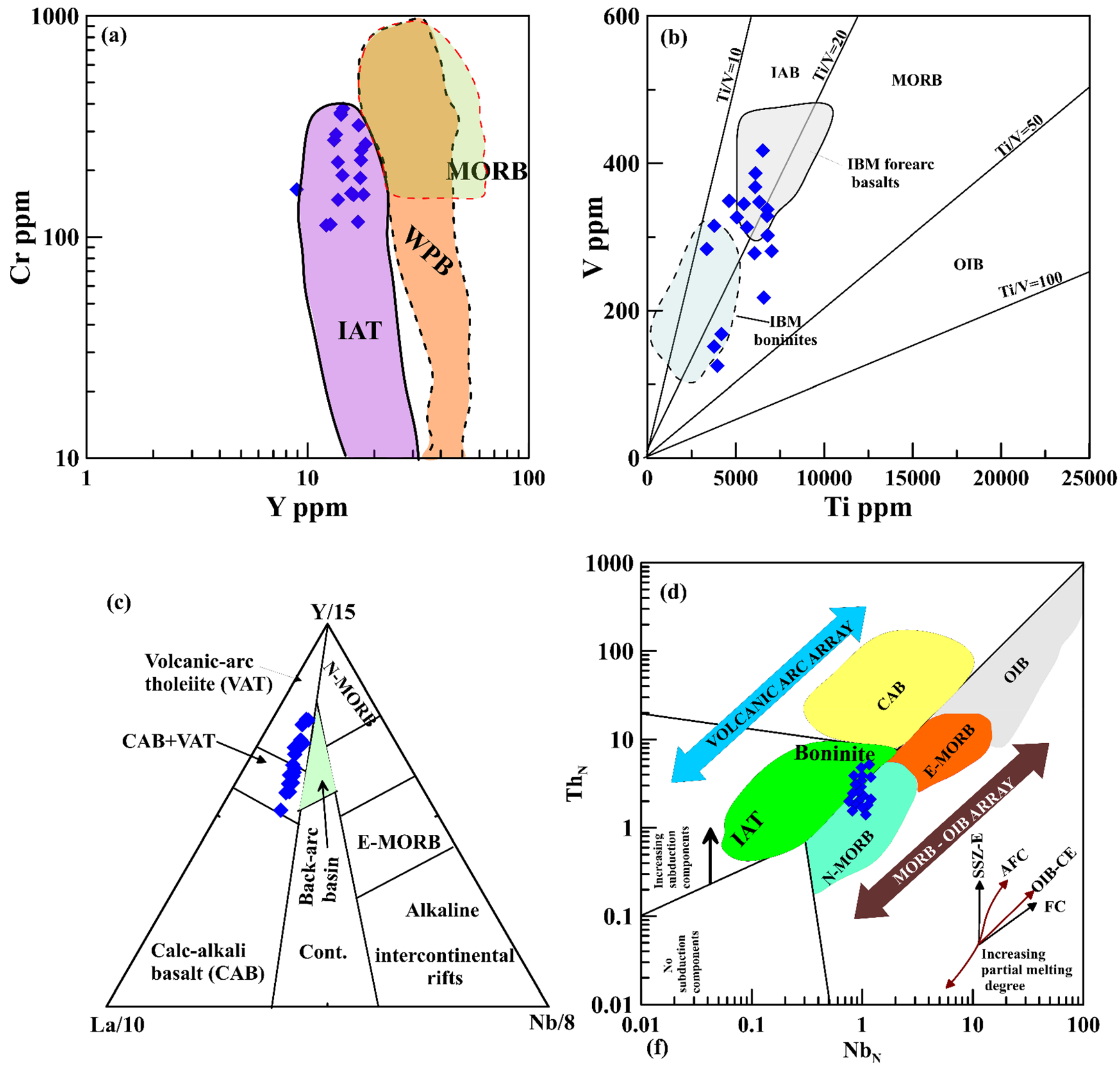

Fig. 12 Plots of the studied MOM rocks on tectonic discrimination: **a** Cr–Y plot (after Pearce 1975), **b** Ti–V discrimination diagram (Shervais 1982). Field of Izu–Bonin–Mariana (IBM) forearc basalts and boninites after Reagan et al. (2010), **c** La–Y–Nb diagram (Cabanis 1989), **d** Th_N versus Nb_N systematic (after Saccani 2015). Normalizing values are the N-MORB composition from Sun and McDonough (1989). *MORB* mid-ocean ridge-basalt, *OIB* ocean island basalt. *N-MORB* normal-type MORB, *E-MORB* enriched-type MORB, *P-MORB* plume-type MORB, *AB* alkaline ocean-island basalt, *SSZ-E* supra-subduction zone enrichment, *AFC* assimilation-fractional crystallization, *OIB-CE* ocean island-type (plume-type) component enrichment, *FC* fractional crystallization

Moreover, the high field strength (HFS) elements (e.g. Ti, Nb, Y, Zr, Hf, Ta, REE) and transition elements (such as Y, V, Ni, Cu) are immobile during the alteration and metamorphic conditions (e.g., Beccaluva et al. 1979; Pearce and Norry 1979). Consequently, the investigated rocks were classified using diagrams that are based on immobile trace elements. Accordingly, MOM samples exclusively plot within the subalkaline basalt on the Zr/TiO_2 versus SiO_2 and Zr/Ti versus Nb/Y diagrams (Figs. 9b and S1b). These plots support the mafic nature of the MOM rocks and indicate that their magma was subalkaline of tholeiitic type. The studied gabbroic rocks are silica-saturated and generally have relatively higher Mg-number (Mg# = 100 Mg/[Mg + Fe]) ranging from 55.91 to 71.35 (Table S5).

The investigated gabbroic rocks have relatively low REE concentrations ranging from 19.18 to 41.41 ppm. The $\sum$REE is gradually increasing from the core of the gabbroic mass towards its outer margins (Table S5). The chondrite-normalizing patterns of the studied rocks (Fig. 9c) are characterized by flat to less fractionated patterns and are slightly enriched in LREE relative to HREE as all the analyzed samples have $(La/Lu)n > 1$ and they possess slightly low positive Eu anomaly [$(Eu/Eu^*)n$ = 1.19–1.62] indicating plagioclase accumulation. The (Eu/Yb)n ratio of the studied MOM is generally > 1 (Table S5), which is higher than MORB (0.37, Thirlwall et al. 1994). In addition, the nearly sub-parallel pattern of middle rare earth element (MREE) to HREE patterns are

Table 1 Results of various amphibole geobarometers of the investigated gabbroic rocks from Gabal Muiswirab area, South Eastern Desert, Egypt

Rock type	Sample no.	Hollister et al. (1987)	P (kbars)	
			Schmidt (1992)	Ridolfi et al. (2010)
Metagabbros	M126/2	2.72	3.30	1.50
		4.21	4.56	1.16
		3.21	3.72	1.80
		2.07	2.76	1.50
	M153/1	2.29	3.10	1.30
		2.30	3.11	1.40
		3.06	3.90	1.60
		2.38	3.17	2.11
		2.09	3.21	0.86
Uralitized gabbro	U12/3	1.22	2.01	0.80
		1.53	2.74	1.20
		2.64	3.23	2.11
		2.94	3.29	2.24
		3.14	3.47	2.87
Flaser metagabbro	F25/1	3.4	3.63	2.44
		4.1	4.61	2.79
		4.2	4.67	2.31
		3.47	4.16	2.14

inconsistent with hornblende fractionation. Thus the hornblende must have been late magmatic (e.g. tschermakite) and or, metamorphic (e.g. magnesio-hornblende). Moreover, the nearly-flat REE patterns of the examined gabbroic rocks (Fig. 9c) are similar to those of N-MORB and match well with ANS ophiolitic metagabbros (e.g., Gahlan et al. 2015; Habtoor et al. 2016; Obeid et al. 2016; Mogahed 2019).

The multi-element spider diagrams normalized to N-MORB (Fig. 9d) show that the MOM is enriched in LILE (particularly Rb, Ba and Sr) and is depleted in many HFS elements (e.g. Nb, Zr, Hf, and Th) which are typical features of subduction-related or altered magmas. The analyzed samples show progressive depletion with increasing compatibility from Nb to Lu (Fig. 9d) which indicated derivation from depleted mantle source or source experienced higher melting degrees (Moghadam et al. 2014). The Rb, Ba, and Pb have the highest values with respect to the other elements reflecting their higher mobility during alteration (Figs. 7 and 9d). The investigated rocks exhibiting slightly negative anomaly for Nb, which represents a striking characterization of the ANS Precambrian mantle rocks (e.g., Maurice et al. 2012; Helmy et al. 2014). Moreover, the negative anomalies of Zr and Nb reflect the clinopyroxene crystallization and amphibole fractionation respectively (Villemant et al. 1981; Pearce 1982). In addition, few samples exhibit slight Ti negative anomalies implying the substantial ilmenite crystallization.

8 Discussion

8.1 Fractional crystallization and insignificant crustal assimilation

The studied MOM samples are characterized by relatively high Mg# with and low contents of Cr and Ni with high FeO^t/MgO ratios (Table S5), which indicates that their parental magma has undergone a higher degree of fractional crystallization. In addition, the positive correlations between Cr, Ni and Mg# (Fig. 10 and Table S5) pointing to the fractional crystallization of olivine and/or clinopyroxene (Fig. 10). In addition, the analyzed metagabbros show a general increase of SiO_2 contents with decreasing FeO^t, MgO and CaO/Al_2O_3, whereas MgO exhibits a positive correlation with compatible elements (e.g., Ni, Sc, Co and V; Table S5), further support the fractionation process of olivine and clinopyroxene. Moreover, the weak variation of CaO, CaO/Al_2O_3 and Sc/Y with increasing Mg# (Fig. 10) coupled with the positive Eu anomaly (Fig. 9c) suggesting plagioclase accumulation (e.g., Naumann and Geist 1999). Moreover, the negative correlation between FeO^t, TiO_2 and P_2O_5, and Mg# (Fig. 10) indicates lesser contribution of $Fe–TiO_2$ oxides and apatite fractionation for MOM magmas. The studied MOM samples exhibiting many evidences that suggest the minimal effect of crustal contamination such as (1) the variation of their Nb/La ratios and Mg# are inconsistent with the trend crustal contamination (Liu et al. 2016; Fig. 10), (2) they exhibit obvious negative Zr and Hf anomalies relative to the N-MORB (Fig. 9d, Liu et al. 2016), (3) they possess higher values of Nb/Ce ratios (0.41–0.88) than those from primitive mantle, average crust and lower crust (0.4, 0.33 and 0.39, respectively; after Taylor and McLennan 1985), and (4) they plot close to the depleted mantle (DMM) and extended towards the OIB Field (Fig. S1c). All these features support that investigated gabbroic rocks were weakly affected by crustal contamination and were derived from a depleted mantle source that experienced a high degree of partial melting similar to Neyriz gabbroic rocks, Iran (Moghadam et al. 2014).

8.2 Mantle source and petrogenesis

The studied MOM exhibiting slightly enrichments of Nb and Ta with depleted contents of Zr and Hf relative to N-MORB (Fig. 9d) which is inconsistent with the source mixing between a depleted mantle and crustal components (Liu et al. 2016). Nielsen and Beard (2000) and Klemme et al. (2006) stated that the fractionation or accumulation of Fe–Ti oxides may result in elevated ratios of Nb, Ta, Zr, and Hf thus, it is valuable to assess this effects on the evolution of the MOM rocks. The analyzed gabbroic rocks exhibit a general increase of FeO^t and TiO_2 with decreasing Mg# suggesting a lesser contribution of fractionation or accumulation of Fe–Ti oxides for the magmas (Fig. 10). Furthermore, the weak variation between Nb/La ratios with increasing TiO_2 further precludes the fractionation of Fe–Ti oxides (Fig. S1d). Accordingly, the slight enrichment of Nb and Ta relative to N-MORB could be considered as primary signatures of the mantle source rather than influenced by fractionation or accumulation of Fe–Ti Oxides or crustal contamination. The enrichments of Nb and Ta for mafic magma could be resulted due to the following mechanisms: (1) partial melting of an OIB type asthenosphere (e.g., Zhou et al. 2009), (2) source mixing of a depleted N-MORB type mantle with OIB like components (Castillo et al. 2007; Castillo 2009; Saccani et al. 2014), or (3) partial melting of a lithosphere mantle metasomatized by OIB-like components (e.g., Wang et al. 2010). Geochemical characteristics of the studied MOM indicate that the first two previously mentioned mechanisms cannot accommodate the petrogenesis of the MOM rocks as these rocks have lower values of Nb/U relative to MORB and OIB (Fig. 11a). Consequently, the geochemical variations of MOM rocks could be from the enrichment of a lithosphere mantle by OIB-like components. Moreover, the ratios of first-row transition elements (e.g., Zn/Fet values; Le Roux et al. 2010, 2011; Murray et al. 2015), could be used to detect the lithological characteristics for the mantle source of the studied gabbroic rocks. The Zn/Fet considered as valuable key for discriminating between peridotite derived melt ($Zn/Fet \times 104 = 9 \pm 1$) and pyroxenite derived melt ($Zn/Fet \times 10^4 = 13$–20). Le Roux et al. (2010) stated that the fractionation of clinopyroxene and Fe–Ti oxides coupled with slab-derived fluids increase the Zn/Fe^t in the mafic melts. Consequently, the fractionation of clinopyroxene is obvious in the MOM rocks (Fig. 11b) but they possess lower Zn/Fe^t values (7.69–12.73; Table S5) relative to pyroxenite-derived melts and more consistent with those rocks that are likely originated from peridotitic mantle source (Fig. 11b). Additionally, the composition and degree of partial melting of the mantle sources for the parental magmas of the mafic rocks could be determined based on the REE abundances and their ratios (Aldanmaz et al. 2000; Zhu et al. 2008). The degree of mantle source depletion of the investigated gabbroic rocks could be assigned using the scheme based on the ratios Sm/Yb and La/Sm (Aldanmaz et al. 2009) and comparing with melting curves obtained using non-modal batch melting modeling (after Bezard et al. 2011; Fig. 11c). Nearly all the analyzed gabbroic samples exhibit a horizontal trend on the diagram (Fig. 11c), suggesting a spinel–lherzolite source (Green 2006; Zhu et al. 2008) and can be accounted for by ~ 5 to 30 % of partial melting of this source at shallow depth which matches with some Egyptian ophiolitic metagabbros (e.g., Ahmed 2013; Gahlan et al. 2015; Obeid et al. 2016; Abdel-Karim et al. 2018; Mogahed 2019).

The contents of some immobile elements (e.g., Zr, Nb, and Yb) in mafic rocks could be used to detect the type of their parent magmas. Pearce and Stern (2006) urged that the comparison of the Nb/Yb ratios reflects the mantle fertility of the mafic rocks. The analyzed gabbroic rocks have Nb/Yb ratios ranging from 0.81 to 1.53 (Table S5), which are higher than those calculated from N-MORB and less than those calculated for E-MORB (0.76 and 3.5 respectively, Sun and McDonough 1989), suggesting derivation from a mixture of enriched and depleted magma sources. According to Leat et al. (2004), the petrogenesis of the mafic rocks could be clearly assisted using the diagram of Th/Yb versus Nb/Yb diagram (Fig. 11d), where Yb used to eliminate the effect of both partial melting and fractional crystallization (Pearce and Peate 1995). The investigated gabbroic rocks plotted scattering in the transition field between mantle array and oceanic arc indicating compositional variation between MORB and IAT, which is a good match with magma originated in supra-subduction zone (SSZ) setting (e.g., Tatsumi and Kogiso 2003; Moghadam et al. 2014; Obeid et al. 2016; Mogahed 2019).

The slightly positive Eu anomaly and the unfractionated REE chondrite-normalized patterns of the investigated gabbroic rocks (Fig. 9c) support that their parental was weakly affected by plagioclase fractionation (e.g., Hermann et al. 2001; Drouin et al. 2009). Moreover, the marked depletion of Zr, Hf, and slightly depletion of Ti (Fig. 9d) coupled with general enrichment of Ba and U for the investigated MOM rocks reflects signature of subduction zone influence which is consistent with ophiolite gabbroic rocks such as Neyriz ophiolite, Iran, Naga Hills ophiolite, India, and Egyptian ophiolites (Moghadam et al. 2014; Dey et al. 2018 and Gahlan et al. 2015; Obeid et al. 2016; Mogahed 2019, respectively). Khedr and Arai (2016) demonstrated that the overall depletion of the HFSE is considered as an eminent feature of the Neoproterozoic sub-arc mantle in Egypt. Consequently, the MOM rocks are characterized by overall enrichments of LILE (e.g., Ba, Pb) over HFSE (e.g., Ti, Nb, Y, Zr, Hf, Ta) (Fig. 9d) suggesting that their parental magma were developed in a sub-arc mantle wedge setting (e.g., Pearce 1982; Tatsumi and Kogiso 2003; Moghadam et al. 2015; Obeid et al. 2016).

The chemical composition of primary clinopyroxene could be used to determine the magmatic affinity of the mafic and rocks originated at different tectonic settings (Leterrier et al. 1982; Beccaluva et al. 1989; Barnes and Roeder 2001; Stern et al. 2004). Most of the analyzed Cpxs from the investigated rocks fall in the field of augite composition (Fig. 4a) and exhibiting higher Si relative to Al (Table S2) suggesting derivation from a tholeiitic melt (Moazzen and Oberhänsli 2008).

8.3 Tectonic setting

Determination of the tectonic setting of metamorphic rocks seems to be difficult as the chemistry of these rocks is modified owing to metamorphism. The tectonic setting of the metamorphic rocks could be traced through elements that thought to be effectively immobile during metamorphisms such as Ti, Y, V, Zr, La, and Nb (Beccaluva et al. 1979; Pearce and Norry 1979). In the Cr versus Y diagram of Pearce (1982), the investigated rocks fall within and the island arc tholeiites (IAT) and extended to the left out of this field (Fig. 12a). Pearce et al. (1984a), ascribed the rocks with similar plots of the studied MOM rocks on the diagram (Fig. 12a) to be of supra-subduction zone tectonic setting. Most of the analyzed gabbroic samples are Ti poor, where TiO_2 wt% ranging from 0.56 to 1.17 (Table S5) and have low Ti/V values (11.84–31.65) consistent with Izu–Bonin–Mariana forearc basalts (Fig. 12b; Shervais 1982). Moreover, the analyzed gabbroic samples are scattered between N-MORB and arc tholeiites fields and none of the samples plot on the back-arc basalts (Fig. 12c) on the triangular diagram suggested by Cabanis (1989). In addition, the scattering plots of the studied MOM rocks between IAT and MORB fields (Figs. 12a, b and S1e-h) indicating that these rocks are consistent with forearc tectonic regime (Beccaluva et al. 2004; Abd El-Rahman et al. 2009; Moghadam et al. 2014; Gahlan et al. 2015; Obeid et al. 2016; Dey et al. 2018; Mogahed 2019). Moreover, the studied metagabbros exhibit high CaO content (Table S5) and depleted REE and HFSE (Fig. 9d) indicating a derivation of Cpx-rich mantle at forearc tectonic setting (Reagan et al. 2010; Mogahed 2019).

Saccani (2015), proposed a discrimination diagram (Fig. 12d) for detecting the tectonic setting of the mafic rocks based on the relation between the contents of Nb and Th; as these two elements are stable during the weathering and low-grade metamorphism (Pearce 2008). On the diagram (Fig. 12d), the studied MOM samples plot in the halfway between MORB–OIB and volcanic arc arrays and clusters between the fields of N-MORB and IAT and exhibiting trend more or less matching with supra-subduction zone (SSZ) trend (Fig. 12d). These observations revealed that the investigated rocks are attributed to intra-oceanic arc settings (Figs. 12a and S1e-h) characterized by a variable contribution from subduction-derived chemical components, such as forearc or back-arc (Saccani 2015). None of the analyzed samples plot into the back-arc field on the diagram (Fig. 12c), hence the possibility of a back-arc tectonic setting will be excluded. Accordingly, the studied MOM rocks are attributed to supra-subduction related magmatism at forearc tectonic setting similar to gabbroic rocks formed in supra-subduction zone magmatism such as Neyriz ophiolite, Iran, Naga Hills ophiolite, India and Egyptian ophiolites (Moghadam et al. 2014, Dey et al. 2018 and Gahlan et al. 2015; Obeid et al. 2016; Mogahed 2019, respectively). Moreover, the chemistry of the analyzed clinopyroxene support forearc tectonic setting as their composition match with those of boninites and IAT (Fig. 4c), where most of boninites are agreed to represent forearcs of interaoceanic arcs (e.g., Beccaluva et al. 2004; Reagan et al. 2010).

Although the Egyptian ophiolites are subjected to numerous studies as they represent the key factor for reconstructing the geodynamic evolution of the Pan-African belt of the ANS, their tectonic setting is still controversial. Earlier studies (e.g., Shackleton et al. 1980; Shackleton 1994; Zimmer et al. 1995) suggested a mid-ocean ridge setting for the Egyptian ophiolites. Recent geochemical studies (e.g., Abdel Aal et al. 2003; Dilek and Ahmed 2003; El-Bahariya and Arai 2003; Farahat et al. 2004; Ahmed et al. 2006; Ahmed 2013) demonstrated a back-arc environment for the Egyptian ophiolites due to their transitional geochemical character, which lie between those of island arcs and MORB. Azer and Stern (2007) attributed the transitional geochemical characters between island arcs and MORB for the Egyptian ophiolites to the transfer of LILE and volatile-rich components from the subduction zone into the overlying mantle wedge. Moreover, there is a general agreement that the Egyptian ophiolites are attributed to Supra-subduction zone ophiolites.

Many authors (e.g., Pearce et al. 1984b; Dilek et al. 1998, 2007; Metcalf and Shervais 2008; Abd El-Rahman et al. 2009) agreed that the supra-subduction zone ophiolites have island arcs geochemical affinities and exhibiting the structure of oceanic crust that resulted from seafloor spreading processes. These ophiolites form during the initial stages of subduction, ridge-trench intersection, and back-arc rifting and spreading (Pearce 2003, 2008). In addition, the subduction initiation is considered as the prominent process through the life cycle of a supra-subduction ophiolite (e.g., Casey and Dewey 1984; Shervais et al. 2004; Dilek and Polat 2008; Abd El-Rahman et al. 2009; Whattam and Stern 2011). With subduction initiation, the early, infant arc magmatism is characterized by depleted arc tholeiitic and boninitic magmas that occur in extensional environments similar to slow spreading centers (e.g., Stern and Bloomer 1992; Bloomer et al. 1995; Robertson 2002; Dilek and Robinson 2003; Cawood et al. 2009). The emplacement of many Phanerozoic ophiolites is generally accompanied by the subduction initiation (Casey and Dewey 1984; Shervais 2001; Reagan et al. 2010). The forearc crust of the Izu-Bonin-Mariana (IBM) arc system in the Western Pacific is a good example of infant-arc formation (Stern and Bloomer 1992; Bloomer et al. 1995; Parkinson and Pearce 1998; Reagan et al. 2010).

The studied MOM rocks are similar to the mafic rocks of (IBM) as they composed mainly of low-Ti tholeiitic rocks (Fig. 9a, b and Table S5) and exhibiting boninitic affinity (Fig. 12b–d) indicating the presence of a highly depleted mantle source that experienced high degree of partial melting (Figs. 11c and S1c; cf., Kurth-Velz et al. 2004; Liu et al. 2017). These characteristics collectively indicating that the studied MOM rocks may have formed in forearc setting during the subduction initiation (cf., Stern and Bloomer 1992; Flower and Dilek 2003; Abd El-Rahman et al. 2009).

The suggested forearc setting of the investigated ophiolitic gabbroic rocks is consistent with the appearance of depleted ultramafic–mafic mantle rocks in the Eastern Desert similar to those rocks from modern forearc tectonic settings (e.g., Azer and Stern 2007; Khalil and Azer 2007; Abd El-Rahman et al. 2009; Farahat et al. 2011; Obeid et al. 2016; Mogahed 2019).

9 Conclusions

The area of Gabal Muiswirab, South Eastern Desert of Egypt consists of a metavolcanic group, mafic rocks (the Muiswirab metagabbros) and granitoids. The metagabbros have ophiolitic affinity. The investigated metagabbros show high Mg# (55.91–71.35); low SiO_2/MgO ratios; high CaO (9.58–12.94 wt%), FeO^t (8.36–12.93 wt%), enrichment of Ni, Cr, and Co with depletion of TiO_2 (0.60–1.64 wt%) and K_2O (0.10–0.41 wt%), nearly unfractionated chondrite-normalized REE patterns; display trace element signatures characterized by the enrichment of LILE over HFSE, comprise low Sm/Yb; Th/Yb and Th/Ta ratios and low Nb contents. These features demonstrated that the investigated metagabbroic represent fragment of older oceanic crust that was generated by 5–30 partial melting of depleted mantle source in a supra-subduction zone environment at forearc tectonic. The geochemical investigation of the studied gabbroic rocks indicated that these rocks are attributed to the ophiolitic metagabbros that suffered from regional metamorphism of low under lower to upper greenschist facies (biotite zone) conditions (at temperature of 450 to 500 °C and pressure of 1–3 kbar) and originated at supra-subduction related magmatism of forearc tectonic setting.

Acknowledgements We express our deep thanks and gratitude to Dr. Galina M. Vovna, Far Eastern Geologic Institute, Russia, for the laboratory facilities and accommodates during the post-doctoral scholarship for the author. Many thanks for Dr. Karabtsov A. Alexandrovich and Ekimova N. Ivanovna (Far Eastern Geologic Institute, Russia), for their help and technical support with the electron microprobe analyses and thin-section preparation. Many thanks to Dr. Abd El Aziem Mehanna for his valuable recommendation and suggestion. Thanks to Dr. Mohammed M. Afife for his help in the field trips. The authors would like to express their deep thanks to editorial team Acta Geochimica, anonymous reviewers and Professor Chuan-Lin Zhang for their efforts, critical comments and constructive reviews that substantially improved the early version of this manuscript.

References

Abd El-Rahman YA, Polat A, Dilek Y, Fryer BJ, El-Sharkawy M, Sakran S (2009) Geochemistry and tectonic evolution of the Neoproterozoic incipient arc–forearc crust in the Fawakhir area, Central Eastern Desert of Egypt. Precambrian Res 175:116–134

Abdel Aal A, Farahat E, Hoinken G, El-Mahalawi M (2003) Ophiolites from the Egyptian Shield: a case for a possible inter-arc origin. Mitt Oesterr Ges 148:81–83

Abdel-Karim A-AM, Ahmed Z (2010) Possible origin of the ophiolites of Eastern Desert, Egypt, from geochemical perspectives. Arab J Sci Eng 35:115

Abdel-Karim A-AM, Ali S, El-Shafei SA (2018) Mineral chemistry and geochemistry of ophiolitic metaultramafics from Um Halham and Fawakhir, Central Eastern Desert, Egypt. Int J Earth Sci 107:2337–2355

Abu El Farh M (2004) A comparative study based on petrography geochemistry of the granitoids in Hafafit area environs, Eastern Desert, Egypt. Ph.D. Dissertation. Suez Canal University, p 169

Abu El-Ela FFA (1997) Geochemistry of an island-arc plutonic suite: Wadi Dabr intrusive complex, Eastern Desert, Egypt. J Afr Earth Sci 24:473–496

Ahmed AH (2013) Highly depleted harzburgite–dunite–chromitite complexes from the Neoproterozoic ophiolite, south Eastern

Desert, Egypt: a possible recycled upper mantle lithosphere. Precambrian Res 233:173–192

Ahmed AH, Hanghøj K, Kelemen PB, Hart SR, Arai S (2006) Osmium isotope systematics of the Proterozoic and Phanerozoic ophiolitic chromitites: in situ ion probe analysis of primary Os-rich PGM. Earth Planet Sci Lett 245:777–791

Akaad M, Noweir M (1980) Geology and lithostratigraphy of the Arabian Desert Orogenic Belt of Egypt between latitudes 25°35′ and 26°30′N. Evolution and mineralization of the Arabian-Nubian shield. Inst Appl Geol (Jeddah) Bull 3(4):127–135

Aldanmaz E, Pearce J, Thirlwall M, Mitchell J (2000) Petrogenetic evolution of late Cenozoic, post-collision volcanism in western Anatolia, Turkey. J Volcanol Geotherm Res 102:67–95

Aldanmaz E, Schmidt M, Gourgaud A, Meisel T (2009) Mid-ocean ridge and supra-subduction geochemical signatures in spinel–peridotites from the Neotethyan ophiolites in SW Turkey: implications for upper mantle melting processes. Lithos 113:691–708

Ali K, Azer M, Gahlan H, Wilde S, Samuel M, Stern R (2010) Age constraints on the formation and emplacement of Neoproterozoic ophiolites along the Allaqi-Heiani Suture, South Eastern Desert of Egypt. Gondwana Res 18:583–595

Azer MK, Stern RJ (2007) Neoproterozoic (835–720 Ma) serpentinites in the Eastern Desert, Egypt: fragments of forearc mantle. J Geol 115:457–472

Bailey SW (1988) Chlorites; structures and crystal chemistry. Rev Mineral Geochem 19:347–403

Barnes SJ, Roeder PL (2001) The range of spinel compositions in terrestrial mafic and ultramafic rocks. J Petrol 42:2279–2302

Beccaluva L, Ohnenstetter D, Ohnenstetter M (1979) Geochemical discrimination between ocean-floor and island-arc tholeiites—application to some ophiolites. Can J Earth Sci 16:1874–1882

Beccaluva L, Macciotta G, Piccardo G, Zeda O (1989) Clinopyroxene composition of ophiolite basalts as petrogenetic indicator. Chem Geol 77:165–182

Beccaluva L, Coltorti M, Giunta G, Siena F (2004) Tethyan vs. Cordilleran ophiolites: a reappraisal of distinctive tectono-magmatic features of supra-subduction complexes in relation to the subduction mode. Tectonophysics 393:163–174

Bezard R, Hébert R, Wang C, Dostal J, Dai J, Zhong H (2011) Petrology and geochemistry of the Xiugugabu ophiolitic massif, western Yarlung Zangbo suture zone, Tibet. Lithos 125:347–367

Bloomer SH, Taylor B, Macleod CJ, Stern RJ, Fryer P, Hawkins JW, Johnson L (1995) Early arc volcanism and the ophiolite problem: a perspective from drilling in the western Pacific. Active margins and marginal basins of the western Pacific, vol 88, pp 1–30

Bodinier J-L, Godard M (2003) Orogenic, ophiolitic, and abyssal peridotites. Treatise Geochem 2:568

Brown E (1977) The crossite content of Ca-amphibole as a guide to pressure of metamorphism. J Petrol 18:53–72

Cabanis B (1989) Le diagramme La/10-Y/15-Nb/8: unoutil pour la discrimination des series volcaniques et la mise en evidence des processus de melande et/ou de contamination crustale. CR Acad Sci Ser II 309:2023–2029

Casey J, Dewey J (1984) Initiation of subduction zones along transform and accreting plate boundaries, triple-junction evolution, and forearc spreading centres—implications for ophiolitic geology and obduction. Geol Soc Lond Spec Publ 13:269–290

Castillo PR (2009) Origin of Nb-enriched basalts and adakites in Baja California, Mexico, revisited: reply. Geol Soc Am Bull 121:1470–1472

Castillo P, Rigby S, Solidum R (2007) Origin of high field strength element enrichment in volcanic arcs: geochemical evidence from the Sulu Arc, southern Philippines. Lithos 97:271–288

Cathelineau M, Nieva D (1985) A chlorite solid solution geothermometer the Los Azufres (Mexico) geothermal system. Contrib Mineral Petrol 91:235–244

Cawood PA, Kröner A, Collins WJ, Kusky TM, Mooney WD, Windley BF (2009) Accretionary orogens through Earth history. Geol Soc Lond Spec Publ 318:1–36

Cox K, Bell J, Pankhurst R (1979) Phase diagrams—introduction. In: The interpretation of igneous rocks. Springer, pp 42–82

Deer W, Howie R, Zussman J (1992) An introduction to the rock-forming minerals, 2nd edn. Longman Scientific & Technical, Harlow, p 696

Dey A, Hussain MF, Barman MN (2018) Geochemical characteristics of mafic and ultramafic rocks from the Naga Hills Ophiolite, India: implications for petrogenesis. Geosci Front 9:517–529

Dilek Y, Ahmed Z (2003) Proterozoic ophiolites of the Arabian Shield and their significance in Precambrian tectonics. Geol Soc Lond Spec Publ 218:685–700

Dilek Y, Polat A (2008) Suprasubduction zone ophiolites and Archean tectonics. Geology 36:431–432

Dilek Y, Robinson PT (2003) Ophiolites in earth history: introduction. Geological Society of London, London

Dilek Y, Moores EM, Furnes H (1998) Structure of modern oceanic crust and ophiolites and implications for faulting and magmatism at oceanic spreading centers. Geophys Monogr Am Geophys Union 106:219–266

Dilek Y, Furnes H, Shallo M (2007) Suprasubduction zone ophiolite formation along the periphery of Mesozoic Gondwana. Gondwana Res 11:453–475

Drouin M, Godard M, Ildefonse B, Bruguier O, Garrido CJ (2009) Geochemical and petrographic evidence for magmatic impregnation in the oceanic lithosphere at Atlantis Massif, Mid-Atlantic Ridge (IODP Hole U1309D, 30 N). Chem Geol 264:71–88

EGSMA (1997) Geologic Map of Jabal Hamatah Quadrangle, Egypt, Scale 1:250000. Ann Geol Surv Egypt 5:1–11

El Gaby S, List F, Tehrani R (1988) Geology, evolution and metallogenesis of the Pan-African belt in Egypt. In: El Gaby S, Greiling R (eds) The Pan-African belt of Northeast Africa and adjacent areas. Friedr Vieweg and Sohn, Berlin, pp 17–68

El Gaby S, List F, Tehrani R (1990) The basement complex of the Eastern Desert and Sinai. The Geology of Egypt. Balkema, Rotterdam, pp 175–184

El Ramly M (1972) A new geological map for the basement rocks in the Eastern and Southwestern desert of Egypt: Scale 1: 1,000,000. Annals of the Geological Survey of Egypt

El Ramly M, Greiling R, Rashwan A, Rasmy AH (1993) Explanatory note to accompany the geological and structural maps of Wadi Hafafit area, Eastern Desert of Egypt. Ann Geol Surv Egypt 9:1–53

El-Bahariya G, Arai S (2003) Petrology and origin of Pan-African serpentinites with particular reference to chromian spinel composition, Eastern Desert, Egypt. Implications for supra-subduction zone ophiolite. In: 3rd international conference on geology of Africa, Assuit, Egypt, pp 371–388

El-Gaby S (2007) Integrated classification and evolution of the Neoproterozoic Pan-African Belt in Egypt. In: The fifth international conference on the geology of Africa, vol 1, pp 143–154

El-Sayed M, Furnes H, Mohamed F (1999) Geochemical constraints on the tectonomagmatic evolution of the late Precambrian Fawakhir ophiolite, Central Eastern Desert, Egypt. J Afr Earth Sci 29:515–533

Farahat E, El Mahalawi M, Hoinkes G, Aal AA (2004) Continental back-arc basin origin of some ophiolites from the Eastern Desert of Egypt. Mineral Petrol 82:81–104

Farahat E, Hoinkes G, Mogessie A (2011) Petrogenetic and geotectonic significance of Neoproterozoic suprasubduction mantle as revealed by the Wizer ophiolite complex, Central Eastern Desert, Egypt. Int J Earth Sci 100:1433–1450

Flower M, Dilek Y (2003) Arc-trench rollback and forearc accretion: 1. A collision-induced mantle flow model for Tethyan ophiolites. Geol Soc Lond Spec Publ 218:21–41

Gahlan HA, Azer MK, Khalil AE (2015) The Neoproterozoic Abu Dahr ophiolite, South Eastern Desert, Egypt: petrological characteristics and tectonomagmatic evolution. Mineral Petrol 109:611–630

Ghoneim M, Takla M, Lebda E (1992) The gabbroic rocks of the central Eastern Desert, Egypt: a geochemical approach. Ann Geol Surv Egypt 18:1–21

Girardeau J, Mevel C (1982) Amphibolitized sheared gabbros from ophiolites as indicators of the evolution of the oceanic crust: Bay of Islands, Newfoundland. Earth Planet Sci Lett 61:151–165

Green NL (2006) Influence of slab thermal structure on basalt source regions and melting conditions: REE and HFSE constraints from the Garibaldi volcanic belt, northern Cascadia subduction system. Lithos 87:23–49

Habtoor A, Ahmed AH, Harbi H (2016) Petrogenesis of the Alaskan-type mafic–ultramafic complex in the Makkah quadrangle, western Arabian Shield, Saudi Arabia. Lithos 263:33–51

Hawthorne FC, Oberti R, Harlow GE, Maresch WV, Martin RF, Schumacher JC, Welch MD (2012) Nomenclature of the amphibole supergroup. Am Mineral 97:2031–2048

He Q, Xiao L, Balta B, Gao R, Chen J (2010) Variety and complexity of the Late-Permian Emeishan basalts: reappraisal of plume–lithosphere interaction processes. Lithos 119:91–107

Hegazy H (1984) Geology of Wadi El-Gemal area, ED, Egypt. Ph.D. Dissertation. Assiut University, p 238

Helmy H (1999) The Um Samiuki volcanogenic Zn–Cu–Pb–Ag-deposit, Eastern Desert, Egypt: a possible new occurrence of cervelleite. Can Mineral 37:143–154

Helmy HM, El-Rahman YMA, Yoshikawa M, Shibata T, Arai S, Tamura A, Kagami H (2014) Petrology and Sm–Nd dating of the Genina Gharbia Alaskan-type complex (Egypt): insights into deep levels of Neoproterozoic island arcs. Lithos 198:263–280

Hermann J, Müntener O, Günther D (2001) Differentiation of mafic magma in a continental crust-to-mantle transition zone. J Petrol 42:189–206

Hollister LS, Grissom GC, Peters EK, Stowell HH, Gisson VB (1987) Confirmation of the empirical correlation of Al in hornblende with pressure of solidification of calc-alkaline plutons. Am Mineral 72:231–239

Huot F et al (2002) The Beimarang mélange (southern Tibet) brings additional constraints in assessing the origin, metamorphic evolution and obduction processes of the Yarlung Zangbo ophiolite. J Asian Earth Sci 21:307–322

Hussein AAA, Ali MM, El Ramly M (1982) A proposed new classification of the granites of Egypt. J Volcanol Geotherm Res 14:187–198

Inoue A, Meunier A, Patrier-Mas P, Rigault C, Beaufort D, Vieillard P (2009) Application of chemical geothermometry to low-temperature trioctahedral chlorites. Clays Clay Minerals 57:371–382

Inoue A, Kurokawa K, Hatta T (2010) Application of chlorite geothermometry to hydrothermal alteration in Toyoha geothermal system, southwestern Hokkaido, Japan. Resour Geol 60:52–70

Jagoutz OE, Burg J-P, Hussain S, Dawood H, Pettke T, Iizuka T, Maruyama S (2009) Construction of the granitoid crust of an island arc part I: geochronological and geochemical constraints from the plutonic Kohistan (NW Pakistan). Contrib Mineral Petrol 158:739

Jiang W-T, Peacor DR, Buseck PR (1994) Chlorite geothermometry? Contamination and apparent octahedral vacancies. Clays Clay Miner 42:593–605

Kawate S, Arima M (1998) Petrogenesis of the Tanzawa plutonic complex, central Japan: exposed felsic middle crust of the Izu–Bonin–Mariana arc. Isl Arc 7:342–358

Khalil A, Azer M (2007) Supra-subduction affinity in the Neoproterozoic serpentinites in the Eastern Desert, Egypt: evidence from mineral composition. J Afr Earth Sci 49:136–152

Khedr MZ, Arai S (2016) Petrology of a Neoproterozoic Alaskan-type complex from the Eastern Desert of Egypt: implications for mantle heterogeneity. Lithos 263:15–32

Klemme S, Günther D, Hametner K, Prowatke S, Zack T (2006) The partitioning of trace elements between ilmenite, ulvospinel, armalcolite and silicate melts with implications for the early differentiation of the moon. Chem Geol 234:251–263

Kocak K, Isık F, Arslan M, Zedef V (2005) Petrological and source region characteristics of ophiolitic hornblende gabbros from the Aksaray and Kayseri regions, central Anatolian crystalline complex, Turkey. J Asian Earth Sci 25:883–891

Kröner A et al (1987) Pan-African crustal evolution in the Nubian segment of northeast Africa. In: Kröner A (ed) Proterozic lithospheric evolution. Geodynamics series, vol 17. American Geophysical Union, Washinngton, pp 235–257

Kurth-Velz M, Sassen A, Galer SJ (2004) Geochemical and isotopic heterogeneities along an island arc–spreading ridge intersection: evidence from the Lewis Hills, Bay of Islands Ophiolite, Newfoundland. J Petrol 45:635–668

Laird J, Albee AL (1981) Pressure, temperature, and time indicators in mafic schist; their application to reconstructing the polymetamorphic history of Vermont. Am J Sci 281:127–175

Le Bas MJ (1962) The role of aluminum in igneous clinopyroxenes with relation to their parentage. Am J Sci 260:267–288

Le Roux V, Lee C-T, Turner S (2010) Zn/Fe systematics in mafic and ultramafic systems: implications for detecting major element heterogeneities in the Earth's mantle. Geochim Cosmochim Acta 74:2779–2796

Le Roux V, Dasgupta R, Lee C-T (2011) Mineralogical heterogeneities in the Earth's mantle: constraints from Mn Co, Ni and Zn partitioning during partial melting. Earth Planet Sci Lett 307:395–408

Leat P, Pearce J, Barker P, Millar I, Barry T, Larter R (2004) Magma genesis and mantle flow at a subducting slab edge: the South Sandwich arc-basin system. Earth Planet Sci Lett 227:17–35

Leterrier J, Maury RC, Thonon P, Girard D, Marchal M (1982) Clinopyroxene composition as a method of identification of the magmatic affinities of paleo-volcanic series. Earth Planet Sci Lett 59:139–154

Lindsley DH (1983) Pyroxene thermometry. Am Mineral 68:477–493

Liou J, Maruyama S, Cho M (1985) Phase equilibria and mixed parageneses of metabasites in lowgrade metamorphism. Mineral Mag 49:321–333

Liu B, Ma C-Q, Guo Y-H, Xiong F-H, Guo P, Zhang X (2016) Petrogenesis and tectonic implications of Triassic mafic complexes with MORB/OIB affinities from the western Garzê-Litang ophiolitic mélange, central Tibetan Plateau. Lithos 260:253–267

Liu X, Xiao W, Xu J, Castillo PR, Shi Y (2017) Geochemical signature and rock associations of ocean ridge-subduction: evidence from the Karamaili Paleo-Asian ophiolite in East Junggar, NW China. Gondwana Res 48:34–49

Loucks RR (1990) Discrimination of ophiolitic from nonophiolitic ultramafic-mafic allochthons in orogenic belts by the Al/Ti ratio in clinopyroxene. Geology 18:346–349

Manya S (2014) Geochemistry of the Palaeoproterozoic gabbros and granodiorites of the Saza area in the Lupa Goldfield, southwestern Tanzania. J Afr Earth Sci 100:401–408

Maurice AE, Basta FF, Khiamy AA (2012) Neoproterozoic nascent island arc volcanism from the Nubian Shield of Egypt: magma genesis and generation of continental crust in intra-oceanic arcs. Lithos 132:1–20

Meschede M (1986) A method of discriminating between different types of mid-ocean ridge basalts and continental tholeiites with the Nb–Zr–Y diagram. Chem Geol 56:207–218

Metcalf RV, Shervais JW (2008) Suprasubduction-zone ophiolites: Is there really an ophiolite conundrum? Spec Pap Geol Soc Am 438:191

Moazzen M, Oberhänsli R (2008) Whole rock and relict igneous clinopyroxene geochemistry of ophiolite-related amphibolites from NW Iran-Implications for protolith nature. J Mineral Geochem 185:51–62

Mogahed MM (2019) Petrogenesis of Zeiatit gabbroic rocks in the Southern Eastern Desert of Egypt: discrimination of arc-related Neoproterozoic gabbros. J Afr Earth Sci 150:239–263

Moghadam HS et al (2014) Supra-subduction zone magmatism of the Neyriz ophiolite, Iran: constraints from geochemistry and Sr–Nd–Pb isotopes. Int Geol Rev 56:1395–1412

Moghadam HS et al (2015) Devonian to Permian evolution of the Paleo-Tethys Ocean: new evidence from U-Pb zircon dating and Sr–Nd–Pb isotopes of the Darrehanjir-Mashhad “ophiolites”, NE Iran. Gondwana Res 28:781–799

Morimoto N, Fabries J, Ferguson AK, Ginzburg IV, Ross M, Seifert FA, Zussman J (1988) Nomenclature of pyroxenes. Mineral Mag 52:535–550

Murray KE, Ducea MN, Schoenbohm L (2015) Foundering-driven lithospheric melting: the source of central Andean mafic lavas on the Puna Plateau (22 S–27 S). Geodynamics of a Cordilleran Orogenic System: The Central Andes of Argentina and Northern Chile: Geological Society of America Memoir 212:139–166

Naumann TR, Geist DJ (1999) Generation of alkalic basalt by crystal fractionation of tholeiitic magma. Geology 27:423–426

Nielsen RL, Beard JS (2000) Magnetite–melt HFSE partitioning. Chem Geol 164:21–34

Nisbet EG, Pearce JA (1977) Clinopyroxene composition in mafic lavas from different tectonic settings. Contrib Mineral Petrol 63:149–160

O’Neill HSC, Jenner FE (2012) The global pattern of trace-element distributions in ocean floor basalts. Nature 491:698

Obeid MA, Khalil AE, Azer MK (2016) Mineralogy, geochemistry, and geotectonic significance of the Neoproterozoic ophiolite of Wadi Arais area, south Eastern Desert, Egypt. Int Geol Rev 58:687–702

Parkinson IJ, Pearce JA (1998) Peridotites from the Izu–Bonin–Mariana forearc (ODP Leg 125): evidence for mantle melting and melt–mantle interaction in a supra-subduction zone setting. J Petrol 39:1577–1618

Pearce J (1975) Basalt geochemistry used to investigate past tectonic environments on Cyprus. Tectonophysics 25:41–67

Pearce JA (1982) Trace element characteristics of lavas from destructive plate boundaries. Andesites 8:525–548

Pearce JA (2003) Supra-subduction zone ophiolites: the search for modern analogues. Special Papers-Geological Society of America, pp 269–294

Pearce JA (2008) Geochemical fingerprinting of oceanic basalts with applications to ophiolite classification and the search for Archean oceanic crust. Lithos 100:14–48

Pearce JA, Norry MJ (1979) Petrogenetic implications of Ti, Zr, Y, and Nb variations in volcanic rocks. Contrib Mineral Petrol 69:33–47

Pearce JA, Peate DW (1995) Tectonic implications of the composition of volcanic arc magmas. Annu Rev Earth Planet Sci 23:251–285

Pearce JA, Stern RJ (2006) Origin of back-arc basin magmas: trace element and isotope perspectives. Geophys Monogr Am Geophys Union 166:63–86

Pearce JA, Harris NB, Tindle AG (1984a) Trace element discrimination diagrams for the tectonic interpretation of granitic rocks. J Petrol 25:956–983

Pearce JA, Lippard S, Roberts S (1984b) Characteristics and tectonic significance of supra-subduction zone ophiolites. Geol Soc Lond Spec Publ 16:77–94

Pearce JA, Barker P, Edwards S, Parkinson I, Leat P (2000) Geochemistry and tectonic significance of peridotites from the South Sandwich arc–basin system, South Atlantic. Contrib Mineral Petrol 139:36–53

Perchuk L (1970) Equilibrium of biotite with garnet in metamorphic rocks. Geochem Int USSR 7:157

Polat A (2012) Growth of Archean continental crust in oceanic island arcs. Geology 40:383–384

Portnyagin M, Danyushevsky L, Kamenetsky V (1997) Coexistence of two distinct mantle sources during formation of ophiolites: a case study of primitive pillow-lavas from the lowest part of the volcanic section of the Troodos Ophiolite, Cyprus. Contrib Mineral Petrol 128:287–301

Pouchou J, Pichoir F (1984) A new model for quantitative x-ray microanalysis. I–application to the analysis of homogeneous samples. Rech Aerosp 3:167–192

Rashwan A (1991) Petrography, geochemistry and petrogenesis of the Migif-Hafafit gneisses at Hafafit mine area, South Eastern Desert, vol 5. Scientific Series of the International Bureau, 0938-7676; 5. Jülich: Forschungszentrum Jülich, c1991, Germany

Reagan MK et al (2010) Fore-arc basalts and subduction initiation in the Izu-Bonin-Mariana system. Geochem Geophys Geosyst 11:1–17

Ridolfi F, Renzulli A, Puerini M (2010) Stability and chemical equilibrium of amphibole in calc-alkaline magmas: an overview, new thermobarometric formulations and application to subduction-related volcanoes. Contrib Mineral Petrol 160:45–66

Robertson AH (2002) Overview of the genesis and emplacement of Mesozoic ophiolites in the Eastern Mediterranean Tethyan region. Lithos 65:1–67

Rudnick R, Gao S (2003) Composition of the continental crust. Treatise Geochem 3:659

Saccani E (2015) A new method of discriminating different types of post-Archean ophiolitic basalts and their tectonic significance using Th–Nb and Ce–Dy–Yb systematics. Geosci Front 6:481–501

Saccani E, Photiades A (2004) Mid-ocean ridge and supra-subduction affinities in the Pindos ophiolites (Greece): implications for magma genesis in a forearc setting. Lithos 73:229–253

Saccani E, Allahyari K, Rahimzadeh B (2014) Petrology and geochemistry of mafic magmatic rocks from the Sarve-Abad ophiolites (Kurdistan region, Iran): evidence for interaction between MORB-type asthenosphere and OIB-type components in the southern Neo-Tethys Ocean. Tectonophysics 621:132–147

Saito S, Arima M, Nakajima T, Kimura J-I (2004) Petrogenesis of Ashigawa and Tonogi granitic intrusions, southern part of the Miocene Kofu Granitic Complex, central Japan: M-type granite in the Izu arc collision zone. J Mineral Petrol Sci 99:104–117

Schmidt MW (1992) Amphibole composition in tonalite as a function of pressure: an experimental calibration of the Al-in-hornblende barometer. Contrib Mineral Petrol 110:304–310

Shackleton RM (1994) Review of Late Proterozoic sutures, ophiolitic mélanges and tectonics of eastern Egypt and north-east Sudan. Geol Rundsch 83:537–546

Shackleton R, Ries A, Graham R, Fitches W (1980) Late Precambrian ophiolitic melange in the Eastern Desert of Egypt. Nature 285:472

Shervais JW (1982) Ti–V plots and the petrogenesis of modern and ophiolitic lavas. Earth Planet Sci Lett 59:101–118

Shervais JW (2001) Birth, death, and resurrection: the life cycle of suprasubduction zone ophiolites. Geochem Geophys Geosyst 2:1010–1045

Shervais JW et al (2004) Multi-stage origin of the Coast Range ophiolite, California: implications for the life cycle of supra-subduction zone ophiolites. Int Geol Rev 46:289–315

Shinjo R, Chung SL, Kato Y, Kimura M (1999) Geochemical and Sr-Nd isotopic characteristics of volcanic rocks from the Okinawa Trough and Ryukyu Arc: implications for the evolution of a young, intracontinental back arc basin. J Geophys Res 104:10591–10608

Singh AK, Khogenkumar S, Singh LR, Bikramaditya R, Khuman CM, Thakur S (2016) Evidence of Mid-ocean ridge and shallow subduction forearc magmatism in the Nagaland-Manipur ophiolites, northeast India: constraints from mineralogy and geochemistry of gabbros and associated mafic dykes. Chemie der Erde-Geochemistry 76:605–620

Staudigel H (2003) Hydrothermal alteration processes in the oceanic crust. Treatise Geochem 3:659

Stern RJ (2018) Neoproterozoic formation and evolution of Eastern Desert continental crust—the importance of the infrastructure-superstructure transition. J Afr Earth Sci 146:15–27

Stern RJ, Bloomer SH (1992) Subduction zone infancy: examples from the Eocene Izu-Bonin-Mariana and Jurassic California arcs. Geol Soc Am Bull 104:1621–1636

Stern RJ, Hedge CE (1985) Geochronologic and isotopic constraints on late Precambrian crustal evolution in the Eastern Desert of Egypt. Am J Sci 285:97–127

Stern RJ, Johnson PR, Kröner A, Yibas B (2004) Neoproterozoic ophiolites of the Arabian-Nubian shield. Dev Precambrian Geol 13:95–128

Sun S-S, McDonough W (1989) Chemical and isotopic systematics of oceanic basalts: implications for mantle composition and processes. Geol Soc Lond Spec Publ 42:313–345

Takla M, Basta E, Fawzi E (1981) Characterization of the older and younger gabbros of Egypt. Delta J Sci 5:279–314

Tatsumi Y, Kogiso T (2003) The subduction factory: its role in the evolution of the Earth's crust and mantle. Geol Soc Lond Spec Publ 219:55–80

Taylor SR, McLennan SM (1985) The continental crust: its composition and evolution. Blackwell Scientific Publications, Oxford, p 312

Thirlwall M, Smith T, Graham A, Theodorou N, Hollings P, Davidson J, Arculus R (1994) High field strength element anomalies in arc lavas: Source or process? J Petrol 35:819–838

Ulrych J et al (1976) Petrology of the petrovice metagabbro. Rozpr Česk Akad Věd Řada Mat Přír Věd 86(9):57

Velde B, Rumble D (1977) Alumina content of chlorite in muscovite-bearing assemblages. Carnegie Inst Wash Yearb 76:621–622

Villemant B, Jaffrezic H, Joron J-L, Treuil M (1981) Distribution coefficients of major and trace elements; fractional crystallization in the alkali basalt series of Chaine des Puys (Massif Central, France). Geochim Cosmochim Acta 45:1997–2016

Wang X-L, Jiang S-Y, Dai B-Z (2010) Melting of enriched Archean subcontinental lithospheric mantle: evidence from the ca. 1760 Ma volcanic rocks of the Xiong'er Group, southern margin of the North China Craton. Precambrian Res 182:204–216

Whattam SA, Stern RJ (2011) The 'subduction initiation rule': a key for linking ophiolites, intra-oceanic forearcs, and subduction initiation. Contrib Mineral Petrol 162:1031–1045

Wilson M (1989) Igneous petrogenesis: a global tectonic approach. Unwin Hyman, London, p 466

Winchester J, Floyd P (1977) Geochemical discrimination of different magma series and their differentiation products using immobile elements. Chem Geol 20:325–343

Winkler HG (2013) Petrogenesis of metamorphic rocks. Springer, Berlin

Workman RK, Hart SR (2005) Major and trace element composition of the depleted MORB mantle (DMM). Earth Planet Sci Lett 231:53–72

Xiao L, Xu Y, Mei H, Zheng Y, He B, Pirajno F (2004) Distinct mantle sources of low-Ti and high-Ti basalts from the western Emeishan large igneous province, SW China: implications for plume–lithosphere interaction. Earth Planet Sci Lett 228:525–546

Xu Y, Chung S-L, Jahn B-m, Wu G (2001) Petrologic and geochemical constraints on the petrogenesis of Permian-Triassic Emeishan flood basalts in southwestern China. Lithos 58:145–168

Yang G, Li Y, Tong L, Wang Z, Duan F, Xu Q, Li H (2019) An overview of oceanic island basalts in accretionary complexes and seamounts accretion in the western Central Asian Orogenic Belt. J Asian Earth Sci 179:385–398

Zhou M-F, Zhao J-H, Jiang C-Y, Gao J-F, Wang W, Yang S-H (2009) OIB-like, heterogeneous mantle sources of Permian basaltic magmatism in the western Tarim Basin, NW China: implications for a possible Permian large igneous province. Lithos 113:583–594

Zhu D et al (2008) Petrogenesis of the earliest Early Cretaceous mafic rocks from the Cona area of the eastern Tethyan Himalaya in south Tibet: Interaction between the incubating Kerguelen plume and the eastern Greater India lithosphere? Lithos 100:147–173

Zimmer M, Kröner A, Jochum K, Reischmann T, Todt W (1995) The Gabal Gerf complex: a Precambrian N-MORB ophiolite in the Nubian shield, NE Africa. Chem Geol 123:29–51